~~SIX-~~MONTH PROGRESS REPORT

on

3 MODIFIED EUTECTIC ALLOYS

FOR HIGH TEMPERATURE SERVICE

to

NATIONAL AERONAUTICS AND SPACE ADMINISTRATION

LEWIS RESEARCH CENTER

Cleveland, Ohio

NASA Grant SC-NsG 639/36-003-033

Prepared by

C. Vishnevsky, S. F. Ramseyer*and J. F. Wallace

Department of Metallurgy

Case Institute of Technology

March, 1967

*Presently with General Electric Company,
Knolls Atomic Power Laboratory, Schenectady, New York

INTRODUCTION

The control of as-cast structures is important for the development of optimum properties of an alloy. This is particularly important in numerous high temperature applications where parts are utilized in the as-cast condition. The present study, now in its third year, has been devoted toward the control of cast structures in order to obtain improved high temperature properties.

In the first year's work the principles of eutectic modification were applied to selected alloy systems offering promise for high temperature service.[1] The results of this investigation demonstrated clearly the marked effect that eutectic modification can exert in producing structures more resistant to stress rupture failure at elevated temperatures. In particular, it was observed that small additions of certain elements, namely titanium, zirconium, carbon and boron substantially alter the structure of Ni-45W, Co-45W, Co-10Al, and Co-37Ta eutectics. Marked improvements were obtained in strength and ductility both at room and elevated temperatures. These improvements in stress rupture and room temperature tensile properties resulted from the breakdown of the normal rod or plate-like eutectic morphologies into more finely divided particulate phases.

The second year's effort was directed toward the cobalt-tungsten and nickel-tungsten systems, since these demonstrated the greatest potential for improvement in stress rupture properties. The objective was to obtain high temperature properties superior to those presently available. An experimental study of the nickel-tungsten and cobalt-tungsten systems indicated that modification with considerable improvement in properties could be achieved with a single addition of .75% Ti, .75% Zr, .5% C, and .1%B. Extensive work was conducted using a Co-35W base composition. The beneficial influence of Ti, Zr, C, and Cr were established; however Mo,V, Ta+Nb and N_2 additions failed to produce this improvement. This work resulted in the development of several Co-35W base alloys exhibiting better stress rupture behavior at 1850°F than the majority of commercially available cobalt base alloys. These results have also been submitted in detailed form to your organization[2].

Some of this improvement is shown in Figures 1 and 2. Figure 1 compares the stress rupture properties of the various compositions studied with the best Co-base alloy developed in a recent NASA publication.[3] Figure 2 compares the better Co-case alloys from this work with those commercial alloys of this type reported in the literature on a strength to weight ratio basis.[4]

The third year's work has been continued in the area of

modification of the above alloys. The effects of relative amounts of Ti, Zr and C on structure and properties were investigated. Furthermore, directional solidification is being applied to a number of alloys to establish the influence of the resultant structures on high temperature properties.

This report describes completed work on the influence of Ti, Zr, and C (Part I (4)) together with the progress to date on the effects of directional solidification (Part II).

Experimental Procedure

The nominal compositions of alloys investigated appear in Table I. These alloys were melted under a modified vacuum induction melting procedure. For the alloys used to establish the effect of Ti, Zr, and C (Part I), these procedures were the same as described in the second annual report (2). Conventionally cast alloys used to study the effect of directional solidification (Part II) were also melted and cast using this procedure with the exception that the unmodified Co-35W and Co-45Walloys were poured under a pressure of 5/6 atmosphere rather than 1/2 atmosphere of argon pressure.

For obtaining directionally solidified structures, the same test bar cluster ceramic shell molds were used as for the conventional castings. The lower portions of these molds were cut off to permit extraction of heat by a water cooled copper chill. The mold and chill were located in an electric resistance furnace capable of operating at 2500°F in vacuo and 2800+ °F in argon. Directionally solidified structures are obtained by pouring metal from an induction furnace into the investment mold inside the electric resistance furnace. Both the induction furnace used for melting and the mold furnace are contained within the atmospheric controlled chamber.

The sides of the mold are maintained at an elevated temperature above the liquidus by the resistance heater. Directionality of the dendritic phases is obtained over most of

the solidifying casting. An example of such a directionally solidified structure is illustrated in Figure 3 for a modified Co-35% W alloy.

The directionally solidified test bar clusters were melted using the procedures employed for conventional castings, however the melts were poured under an argon pressure of 5/6 atmospheres to minimize decomposition of the electric resistance furnace heating elements.

Constant load stress rupture tests were conducted at 1800°F and 1850°F. In Part I, only ductility and time to fracture were determined. In Part II, creep strain was also measured by means of dial gages attached to the weighted end of the stress rupture rack loading arms. Slippage of the specimens in the grips during seating probably introduced some error initially. It is believed that, except for these initial inaccuracies, the curves of creep strain versus time from which minimum creep rates were determined are reliable.

Metallographic examination was conducted on both as cast and tested stress rupture specimens. The mechanically polished structures were etched with a modified Fry's etch consisting of 50 parts HCl, 25 parts HNO_3, 1 gram $CuCl_2$-$2H_2O$, and 150 parts water.

Results and Discussion

PART I: Influence of Ti, Zr, and C on Structure and Properties.

Microstructural Considerations:

A special series was cast to determine the specific influence of Ti, Zr and C on the cast structure and properties of a Co-35W-3Cr base alloy. Figures 4-12 show the microstructures of these alloys. Photomicrographs marked "after-testing" are of samples cut from the gage length of specimens tested in air at 1850°F and 20,000 psi initial load. The structure of these alloys etched more readily and for this reason these structures usually appear darker. The atom ratio of the Ti + Zr to C added was shown to have a major influence on both the types and morphology of phases which occurred in the as-cast structures. A continuous interdendritic network of the M_6C carbide, Co_3W_3 C or phase in a "chinese script" pattern, formed when only C was added to the base alloy, as shown in Figures 4 and 8. The morphologies of the M_6C were similar in the two alloys, with the volume percent of the carbide phase increasing approximately 50% as the C level was raised from 0.5 to 1. The considerably finer dendritic structure for the 0.5C alloy resulted because of the lower pouring temperature for this heat, 150°F superheat compared to the usual 300°F. With the addition of Ti, Zr and C in a ratio less than approximately 0.5 as exemplified by the alloys with 2Zr-1C and 2Ti-1C, Figures 9 and 10 respectively, the M_6C network is still

continuous though reduced in volume. The MC's have formed in varying amounts and are present in greater amounts in the 2Ti-1C alloy with a ratio of 0.5 than in the 2Zr-1C alloy with a ratio of 0.26.

By increasing the ratio beyond 0.5, the M_6C network is partially or completely broken up. At a ratio of 0.53 for the 2 Zr-0.5C alloy, the M_6C particles are only partly dispersed, Figure 5. At a ratio of 0.76, as for the 1Ti-1Zr-.5C alloy in Figure 11 and the 2 Ti-2Zr-1C alloy in Figure 12, the M_6C network is completely broken up with faceted particles of the MC carbides randomly mixed with the fine, equiaxed M_6C carbide particles. The only differences between the two structures are the slight increase in the volume percent of second phases and the larger, more idiomorphic MC particles in the latter alloy.

If the ratio is increased still further to a stoichiometric addition of Ti+Zr to C of 1, as illustrated by the 2Ti-0.5C alloy shown in Figure 6, the structure has a very high percentage of MC carbides and only a few random particles of a third phase that is assumed to be the M_6C. With the increase in the ratio to approximately 1.5 for the 2Ti-2Zr-0.5C alloy shown in Figure 7, a large excess of Ti+Zr exists and a bulky new phase forms, probably a (Ti,Zr) Co_3 compound (5). Interspersed with these were smaller faceted particles, probably MC carbides. However, these phases were not definitely established.

At a given C level the MC carbides will form at the expense of the M_6C carbides, since these are the more stable phase thermodynamically. Since the molar volume of the M_6C phases would be expected to be considerably larger than that for the MC phases, the decrease in the volume fraction of the second phases observed with an increasing Ti+Zr to C ratio (see Table II) at a constant C level probably reflects this change in the amounts of M_6C and MC phases formed.

The variation in as-cast grain size of this series of alloys, as presented in Table II, was very erratic. The majority of the alloys had a grain size of from 10-15 grains per 1/4 inch diameter for the 0.5C alloy was probably due to the lower pouring temperature of this heat; the cause of the very small grain size of approximately 40 grains per diameter for the 2Ti-0.5C could not be definitely established. Titanium is known to be a very effective grain refiner for certain cast steels (6) and perhaps, when added singularly to this Co-base alloy, it acts in a similar manner. It should also be noted that the grain size of 2-4 and 6-8 grains per diameter for the two heats of the 2Ti-2Zr-1C alloy was slightly coarser than for the other alloys.

The influence of Ti, Zr and C on the microstructure of the Co-35W-3Cr base alloy after exposure to 1850°F is shown by comparing the various "after-testing" microstructures. When the M_6C carbide was a continuous interdendritic network, Figures 4, 8-10, no noticeable precipitation of the Co_3W phase was evident

in the "after-testing"structures. The amount and coarseness of the Co_3W precipitation after exposure at 1850°F increased as the Ti+Zr to C ratio was increased as indicated by the "after-testing" structures presented in Figures 5-7,12. The structures of these latter alloys exhibited smaller amount of M_6C, larger amounts of the MC phases and a broken up M_6C network. The morphology and size of the carbide phases were generally unchanged after testing at 1850°F. The differences in response of the matrices to exposure to elevated temperatures is probably caused by the influence of Ti and Zr on the amount of W in solid solution in the Co matrix. Without the addition of Ti and Zr, sufficient W is tied up by the formation of the M_6C phase network to lower the W dissolved in the matrix below the level at which Co_3W will form and precipitate at 1850°F. This appears to be true as long as the M_6C carbide network is continuous. However, when the Ti plus Zr level is increased to the level where the M_6C carbide network is broken up, i.e., carbon is tied up as MC and the M_6C does not form in as large quantities, the matrix becomes supersaturated in W, and Co_3W precipitates during testing at 1850°F. The progressive coarsening of the matrix precipitate with increasing Ti+Zr to C ratio is shown by comparing the "after-testing" structures illustrated in Figures 5-7. The particularly heavy precipitation noted in the 2Ti-2Zr-1C alloy (Figure 12) was probably caused in part by the longer time at elevated temperature.

Stress Rupture Properties of Co-35W Base Alloys:

The stress rupture curves for the various alloys tested are presented in Figures 13 and 14. Table III (a) lists both time to fracture and reduction in area at the different levels of initial stress. The calculation of reduction in area was questionable in some cases because of the anisotropic nature of the fracture cross section or extensive oxidation of the test specimen. These values have been marked either (a) or (o) in Table III.

The results of the investigation into the effect of Ti, Zr and C additions to a Co-35W-3Cr base material are presented by separating the alloys into two groups by C level: 0.5C level alloys shown in Figure 13 and 1.0C level alloys in Figure 14. The two alloys with only C added had the poorest stress rupture lives, as would be expected from the continuous interdendritic carbide network in their microstructures (Figure 4 and 8). Although these alloys exhibited extensive void formation and cracking along the full gage length after testing, both had substantial ductility, approximately 50% reduction in area for the alloy with 0.5C and 20-25% reduction in area for the alloy with 1.0C. The large reductions in area for the alloys during stress rupture testing is probably caused by the effect of the carbide network on the W content and distribution in the Co matrix. With the formation of a continuous network of the M_6C sufficient tungsten is tied up so Co_3W cannot form during testing and a low W zone probably exists

near the matrix-carbide interface. Thus, the matrix and particularly the interface is relatively weak so extensive deformation and grain boundary sliding occurred. The extensive interface deformation would also account for the larger number of voids and cracks which formed during the testing of these alloys.

The atomic ratio of Ti plus Zr to C was found to be a more significant factor in correlating the influence of alloy content on properties than either weight or atomic percent of Ti, Zr and/ or C added. As the ratio increased the stress rupture life increased initially, then decreased when the ratio was equal to or greater than one. The importance of the ratio probably results from its effect on the type of carbides and morphology that forms. As the ratio increases from 0 to about 1/2, the continuous network of the M_6C carbide forms in increasingly smaller amounts and finer size, with a certain amount of MC carbides occurring. The properties for the 2Zr-1C (ratio-0.26) and 2Ti-1C (ratio-0.50) alloys shown in Figure 14 illustrate the influence of these changes in microstructure. The modest improvement in properties for the 2Zr-1C alloy above those for the 1C alloy is probably caused by the tying up of some of the C as ZrC. Thus, less M_6C forms, more W is in solid solution, so the matrix and particularly the interface region is strengthened. Further improvement in properties resulted when more C is tied up in the 2Ti-1C alloy.

Both of these alloys had substantial elevated temperature ductility (reductions in area of approximately 40-50%) with void and crack formation along the full gage length. This behavior is similar to that observed for the 1C alloy.

As the ratio increases further from 1/2 to 1, the M_6C network is broken, the particles become more rounded and equiaxed and appear in decreasing amounts, and the MC carbides increase in amount and size. These changes in microstructure are reflected in the slightly improved properties for the 2Zr-0.5C and 2Ti-0.5C alloys at 20,000 psi, Table III (a). The analysis of these alloys is complicated by the observed accelerated oxidation for the 2Zr-0.5C alloy, and the very fine grain size of the 2Ti-0.5C alloy. Both these factors tend to lower the stress rupture properties of a material by causing premature failures at lower stress levels, and longer testing times. Thus, the improved life of both these alloys at the higher stress of 20,000 psi is nullified at the lower stress of 15,000 psi and the slopes to their stress rupture curves are steeper, Figure 13. At still higher ratios, with Ti plus Zr in excess of the stoichiometric amount needed to form the MC carbides, a new phase forms which weakens the material. The detrimental effect of excess Ti plus Zr is shown by comparing the stress rupture curve of the 2Ti-2Zr-0.5C alloy (ratio-1.53) with that of the standard 1Ti-1Zr-0.5C (ratio-.76) in Figure 13.

A ratio slightly less than one appears to be optimum judging by the excellent properties of the standard and Co-35W-3Cr-2Ti-2Zr-1C-0.1B alloys, both with ratios of 0.76. The better properties of the latter over the former shows the effect of increased amounts of Ti, Zr and C and indicates that still larger additions might increase stress rupture life further. A point of diminishing returns exists because the structure becomes overloaded with carbides and the oxidation rate increases at higher Ti and Zr contents.

PART II Effect of Directional Solidification

Microstructure:

The microstructures for all alloys investigated in Part II appear in Figures 15 to 18. Conventionally cast material in most cases had the same structures as observed in previous phases of this project (2,4). Figure 15 (a) shows the microstructure of the Co-35W- .05 Zr alloy. Although the structure was not appreciably modified by the addition of this small quantity of Zr, its etching characteristics were altered. The intergranular Co_3W precipitate is not so well defined as in earlier work in which Zr was not added. Figure 15 (b) shows a longitudinal section of this alloy solidified directionally. The Co_3W is well defined and appears to lie interdendritically parallel to the direction of solidification.

The structure of conventionally cast Co-35W-3Cr-2Ti-2Zr-1C-.1B is shown in Figure 16 (a), and was identical with that obtained previously (2,4), see Figure 12. The carbides and small regions of carbide eutectic are randomly distributed. Not only was the structure changed so that it appeared directional, but the distribution and appearance of second phases changed drastically. The carbide eutectic is much coarser and more evident in the directional casting. The blocky M_6C carbides became less randomly distributed and clustering of these was observed.

The structure of the unmodified Co-45W-.05 Zr alloy is shown in Figures 17 (a) and 17 (b). Both the conventional

and directionally solidified castings are entirely eutectic. In the directional casting primary dendrites of Co are aligned in the direction of solidification. Secondary dendrite arms of Co and lamellae of W_6Co_7 lie nearly perpendicular to the direction of solidification.

The modification of the Co-45W eutectic composition resulted in a considerably less acicular microstructure. The conventionally cast material, Figure 18 (a), contains thick platelets of W_3C0_3C and globular MC carbides (7). Directional solidification of this alloy coarsened the structure and aligned the W_3Co_3C perpendicular to the direction of solidification, Figure 18 (b).

Stress Rupture Properties:

The results of all stress rupture tests are listed in Table III (b). In general, ductility in the stress rupture test, as measured by per cent elongation, was increased by directional solidification. The average increase in ductility ranged from 20% for Co-35W-3Cr-2Ti-2Zr-1C-.1B to 78% for the Co-45W unmodified alloy. The reverse effect was obtained for modified Co-45W with the ductility decreasing 72% on directional solidification.

Stress rupture curves for the various alloys and conditions appear in Figures 19 to 22. A pronounced improvement in stress rupture life resulting from directional solidification was obtained for unmodified Co-35W, Figure 19. For modified

Co-35W, Figure 20, the directional structure exhibited lower stress rupture lives. This behavior is attributed at least partly to the clusters of carbides at which cracks initiated. The variation of minimum creep rate for these alloys is consistent with differences in stress rupture life. Figure 23 shows that directional solidification of unmodified Co-35W increased creep resistance as reflected in a decrease in minimum creep rate. For modified Co-35W the minimum creep rate is greater for the directionally solidified structure, consistent with lower stress rupture lives, Figure 24.

The behavior of the Co-45W base composition was more complex. On directional solidification, the stress rupture life of the modified alloy was improved at low stresses, but decreased at high stresses, Figure 21. Two straight line portions may provide the best description of these data. The minimum creep rate shows a similar cross over, Figure 25. At low stresses the rate is lower for the directional castings. The results for the unmodified Co-45W alloy exhibit similar, though less well defined behavior. The stress-life curves, Figure 22, show a tendency for improved lives, over conventionally cast material, with decreasing stress for the directional specimens. Similarly the minimum creep rate decreases more rapidly with decreasing stress for this structure, Figure 26.

The tendency for the directional structures to possess improved lives at lower stresses was noted by VerSnyder and Guard (8). The possible variation of fracture mode with stress is currently being examined. Preliminary metallographic examination of broken specimens indicates a strong influence of grain boundary and second phase orientation on fracture behavior. In some cases, the beneficial effects of transverse grain boundary elimination sometimes conflict with the unfavorable alignment of second phases. For example, in the Co-45W modified alloy, solidified directionally, the W_3CO_3C lies perpendicular to the loading direction. Voids initiated at these internal notches, propagating transgranularly. It appears that at higher stresses, this stress concentration effect overshadowed the favorable alignment of grain boundaries thus leading to poorer stress rupture properties.

SUMMARY

Part I

Using a base alloy of Co-35W-3Cr, it was found that the atomic ratio of Ti plus Zr to C determined both the type and morphology of the second phases that formed. As the ratio increased from 0 to approximately 1/2, a continuous network of M_6C carbides with increased MC carbides occurred; above 1/2 to 1 the M_6C network was broken up, the particles becoming

rounder and more equiaxed, and an increasing percent of MC carbides formed; and above 1, MC carbides and a new phase were observed.

The atomic ratio of Ti and Zr to C also affected stress rupture properties considerably. Optimum results were obtained with a ratio of .76. Two alloys based on this ratio, Co-35W-3Cr-0.1B with additions of 1Ti-1Zr-0.5C and 2Ti-2Zr-1C had stress rupture lives which compare very favorably with commercial Co-base alloys.

Part II:

Directional solidification of four Co-W base alloys exerted a complex influence on structure and stress rupture behavior. In the Co-35W unmodified alloy the structure was aligned axially in the stress rupture specimens and properties were enhanced over the entire range of stress investigated.

For Co-45W, both modified and unmodified, conventionally cast specimens exhibited longer lives at high stresses, but at low stresses the directionally solidified structures were superior. In these alloys the major second phases were aligned perpendicular to the specimen axis, while the grain boundaries were oriented longitudinally.

In the Co-35W modified alloys directional solidification altered considerably the shape and distribution of microconstituents leading to a reduction in stress rupture life.

FUTURE WORK

Attempts will be made to produce directionally solidified Co-35W-3Cr-2Ti-2Zr-1C-.1B in which carbides are not clustered. It is expected that the stress rupture specimens machined from directional ingots of this alloy will be more homogeneous because of concentration of carbides near the surface.

The role of prior cast structure on hot workability and properties after hot working is to be examined for both modified and unmodified alloys. Ingots conventionally cast in warm zircon molds are currently being produced. Directionally solidified ingots will soon be cast in a manner similar to that used for the test bar clusters.

REFERENCES

1. R. L. Ashbrook and J. F. Wallace "Modification of Eutectic Alloys for High Temperature Service". Trans. A.I.M.E., Vol. 236, 1966, pp. 670-678.

2. S. F. Ramseyer and J. F. Wallace, "Second Year Interim Technical Report on NASA Grant SC-NsG-639", June 1966.

3. T. C. Freche, R. L. Ashbrook and G. D. Sandrock, "The Potential for Cobalt-Tungsten Superalloys" Metal Progress, May, 1965, p. 74.

4. S. F. Ramseyer "Effect of Solidified Structure on Properties of Superalloys" Ph.D Thesis. Case Institute of Technology 1966.

5. Wagner, H. T. and Hall, A.M.,"The Physical Metallurgy of Cobalt-Base Superalloys-DMIC Rpt. 171, Af 33. (616)- 7747, July 6, 1962, Columbus, Ohio.

6. Church, N., Wieser, P. and Wallace, J. F. "Control of Cast Grain Size of Steel Castings, Effect of Grain Refinement and Properties" Trans. AFS., Vol. 74, 1966, pp. 113-128.

7. Rautala, P. and Norton, J. T. "Tungsten-Cobalt-Carbon System. Trans. A.I.M.E., Vol. 194, 1956, pp. 1045-1050.

8. F. L. Ver Snyder and R. W. Guard, "Directional Grain Structures for High Temperature Strength" Trans. ASM., Vol. 52, 1960, p. 485.

TABLE I. - NOMINAL COMPOSITION OF ALLOYS INVESTIGATED

(Weight Percent)

Part I

Co-35W-3Cr-0.5C-0.1B
Co-35W-3Cr-2Ti-0.5C-0.1B
Co-35W-3Cr-2Zr-0.5C-0.1B
Co-35W-3Cr-2Ti-2Zr-0.5C-0.1B
Co-35W-3Cr-1C-0.1B
Co-35W-3Cr-2Ti-1C-0.1B
Co-35W-3Cr-2Zr-1C-0.1B
Co-35W-3Cr-1Ti-1Zr-0.5C-0.1B
Co-35W-3Cr-2Ti-2Zr-1C-0.1B

Part II

Co-35W-.05Zr
Co-35W-3Cr-2Ti-2Zr-1C-0.1B
Co-45W-.05Zr
Co-45W-.75Ti-.75Zr-.25C-0.1B

TABLE II - QUANTITATIVE METALLOGRAPHIC DATA FOR SEVERAL Co-35W BASE ALLOYS IN PART I.

Alloy Composition (Nominal-Wgt.%)	Atomic Ratio Ti+Zr/C	Grain Size, Grains per 1/4"-Dia.	Total Vol. Fraction of Second Phases	Mean Free Path, Microns	Time to Fracture at 1850°F and 15,000 psi, Hours
Co-35W-3Cr-1Ti-1Zr-.5C-.1B					
A.)	.76	7-10	21.0	20.1	154.2
B.)	.76	12-16	20.8	21.2	131.9
C.)	.76	9-12	20.1	19.9	144.3
D.)	.76	15-20	21.0	20.7	150.7
Co-35W-3Cr-.5C-.1B	0	15-20	32.5	10.8	6.3
Co-35W-3Cr-2Zr-.5C-.1B	.53	8-12	28.5	24.2	35.7
Co-35W-3Cr-2Ti-.5C-.1B	1.0	40	22.1	24.4	31.3
Co-35W-3Cr-2Ti-2Zr-.5C-.1B	1.5	10-15	21.8	27.2	46.0
Co-35W-3Cr-1C-.1B	0	10-15	48.0	21.4	1.4
Co-35W-3Cr-2Zr-1C-.1B	.26	10-15	37.0	26.5	8.1
Co-35W-3Cr-2Ti-1C-.1B	.50	10-15	36.0	28.8	5.8
Co-35W-3Cr-2Ti-2Zr-1C-.1B					
A.)	.76	2-4	24.0	19.3	224.9
B.)	.76	6-8	22.5	17.4	171.7

Table III - RESULTS OF STRESS RUPTURE TESTS IN AIR AT 1800 and 1850°F.

a) Results for Part I (All tests at 1850°F)

Alloy Composition (Nominal-Wgt.%)	Initial Stress, Psi	Time to Fracture, Hours	Reduction in Area, Percent	
Co-35W-3Cr-1Ti-1Zr-.5C .1B *	15,000	145.2	--	(0)
	17,500	61.7	--	
	20,000	29.5	--	
	22,500	17.6	--	
	25,000	11.5	--	
* Avg. of 5 heats. Heats listed individually, Table VI (ref.2)				
Co-35W-3Cr-.5C-.1B	15,000	6.3	51.8	
	17,500	3.3	55.2	
	20,000	2.0	46.3	
Co-35W-3Cr-2Zr-.5C-.1B	15,000	35.7	89.7	(0)
	17,500	19.3	69.6	(0)
	20,000	12.0	84.6	(0)
Co-35W-3Cr-2Ti-.5C-.1B	15,000	31.3	37.2	
	17,500	18.5	39.1	
	20,000	13.2	30.9	

(A) Anistropic deformation, assumed ellipsoidal fracture cross-section

(0) Heavy Oxidation

TABLE III - Continued. RESULTS OF STRESS RUPTURE TESTS IN AIR AT 1800 and 1850°F.

Alloy Composition (Nominal-Wgt.%)	Initial Stress, Psi	Time to Fracture, Hours	Reduction in Area, Percent
Co-35W-3Cr-2Ti-2Zr--.5C-.1B	15,000	46.0	18.2
	17,500	28.5	30.8
	20,000	23.0	16.2
Co-35W-3Cr-1C-.1B	15,000	1.4	29.8
	17,500	0.7	14.8
	20,000	0.3	46.0
	20,000	0.4	15.1
Co-35W-3Cr-2Zr-1C-.1B	15,000	8.1	40.0
	17,500	5.4	40.0
	20,000	2.3	23.0
Co-35W-3Cr-2Ti-1C-.1B	15,000	36.1	55.7
	17,500	12.8	65.2
	20,000	5.8	26.8
Co-35W-3Cr-2Ti-2Zr-1C-.1B	15,000	224.9	29.2(A) (0)
	15,000	171.7	22.2(A) (0)
	17,500	117.1	37.8
	17,500	70.7	24.4
	20,000	42.5	41.2(A)
	20,000	44.8	34.8
	25,000	14.9	28.9
Co-35W-3Cr-1Ti-1Zr-.5C	15,000	52.0	7.0
	17,500	29.8	2.5
	20,000	20.4	4.8
	25,000	8.0	8.7

(A) Anistropic deformation, assumed ellipsoidal fracture cross-section

(0) Heavy Oxidation

Table III, (continued)

b) Results for Part II

Alloy Comp. (Nominal Wt.%)	Temp. °F	Initial Stress Psi	Time to Fracture, Hours	% Elongation	Minimum Creep Rate, 10^{-3} in/in/hr.
Co-35W-.05 Zr (conventional)	1800	12,500	49.8	8.8	.952
	"	15,000	45.9	10.4	1.37
	"	17,500	15.9	16.0	6.43
	"	20,000	7.5	12.0	10.3
	"	25,000	1.8	8.8	48.0
Co-35W-.05Zr (Directional)	1800	15,000	69.5	12.0	N.D.*
	"	15,000	128.1	16.0	N.D.
	"	15,000	63.2	11.2	1.21
	"	20,000	23.7	12.0	5.20
	"	25,000	6.3	17.6	31.2
Co-45W-.05 Zr (conventional)	1800	10,000	12.2	8.0	3.75
	"	15,000	3.7	5.6	14.3
	"	20,000	1.7	7.2	48.0
Co-45W-.05 Zr (Directional)	1800	10,000	12.5	17.6	4.56
	"	12,500	4.8	10.4	12.9
	"	15,000	2.5	14.4	16.5
	"	20,000	.40	8.0	120
	"	20,000	.35	11.2	111
Co-45W-Ti- -.75 Zr-.25C-.1B (Conventional)	1800	12,500	55.1	21.6	1.2
	"	15,000	37.8	16.8	1.83
	"	17,500	30.1	19.2	2.86
	"	20,000	21.5	17.6	N.D.
Co-45W-.75 Ti - -.75 Zr- .25C-.1B (Directional)	1800	12,500	81.9	6.4	.315
	"	15,000	55.9	7.2	.908
	"	17,500	24.3	5.6	1.78
	"	20,000	3.1	4.0	5.80
	"	20,000	5.9	3.2	7.56
Co-35W-3Cr-2Ti- -2 Zr- 1C- .18 (Conventional)	1850	17,500	70.9	23.2	1.61
	"	17,500	88.7	34.4	N.D.
	"	20,000	51.4	28.8	N.D.
	"	25,000	17.0	24.0	13.3
Co-35W-3Cr-2Ti -2Zr-1C-.1B (Directional)	1850	15,000	126.6	41.6	.784
	"	17,500	71.6	32.8	N.D.
	"	20,000	27.7	27.2	3.78
	"	25,000	9.1	30.4	14.6

*N.D. - Not Determined

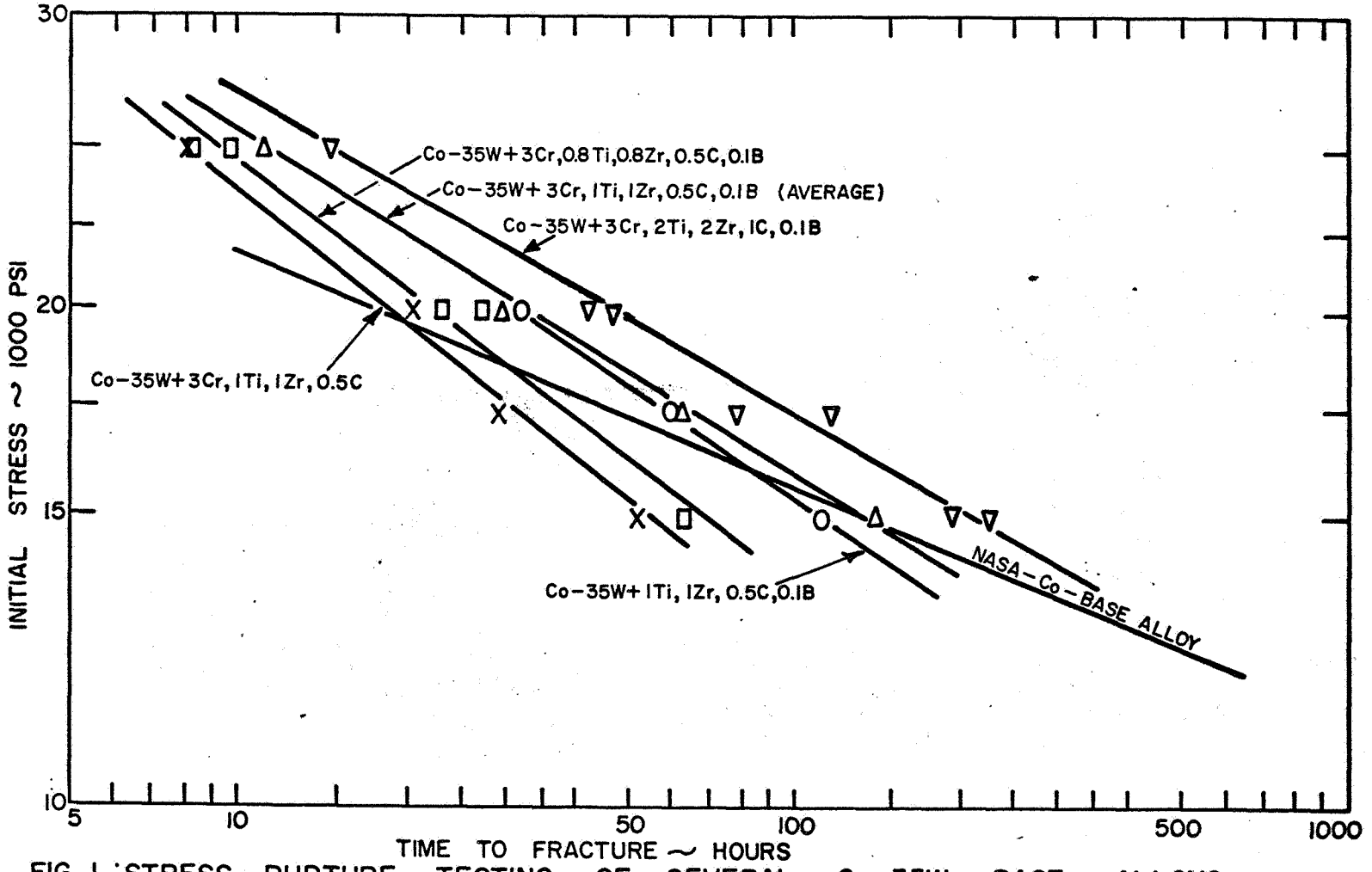

FIG. 1 : STRESS-RUPTURE TESTING OF SEVERAL Co-35W BASE ALLOYS. (TESTED AT 1850°F IN AIR)

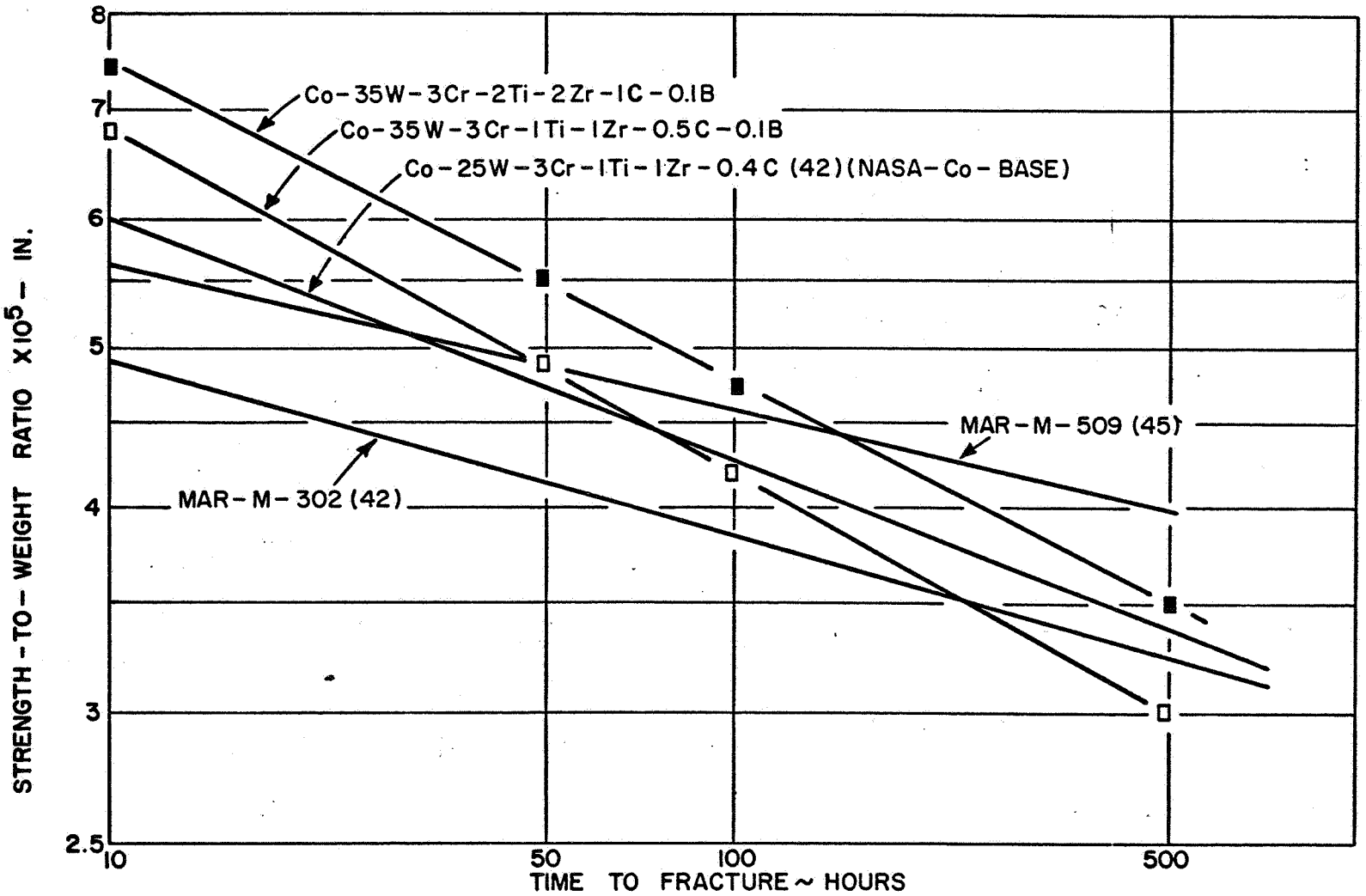

FIGURE 2 : STRESS-RUPTURE PROPERTIES OF SEVERAL Co-BASE SUPERALLOYS ON A STRENGTH-TO-WEIGHT RATIO BASIS.(TESTED AT 1850°F IN AIR)(FROM REF. 4)

Location of Chill

Figure 3. Longitudinal view of gage section in directionally solidified stress rupture specimen of Co-35W-3Cr-2Ti-2Zr-1C-.1B. approx. 9X magnification.

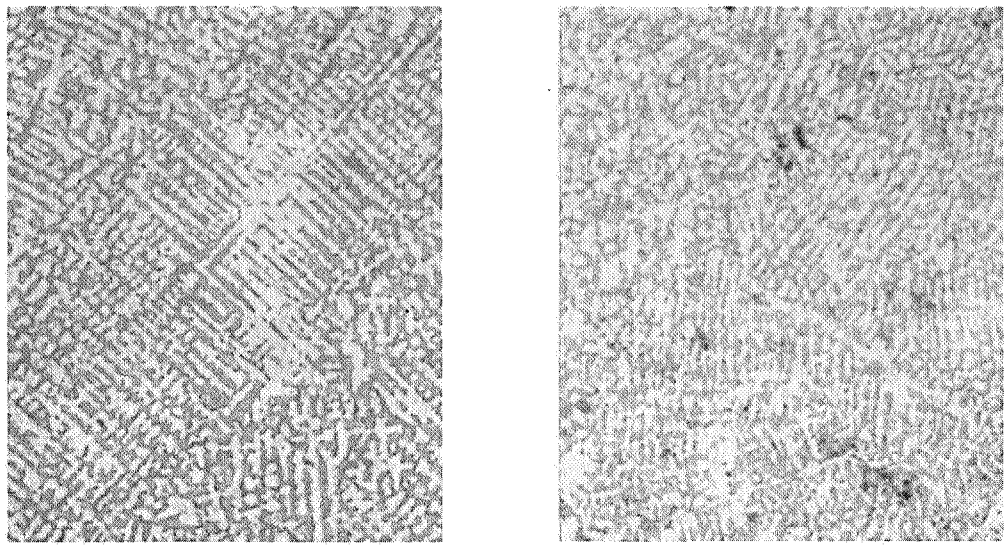

100X

a) As-cast

100X

b) Tested

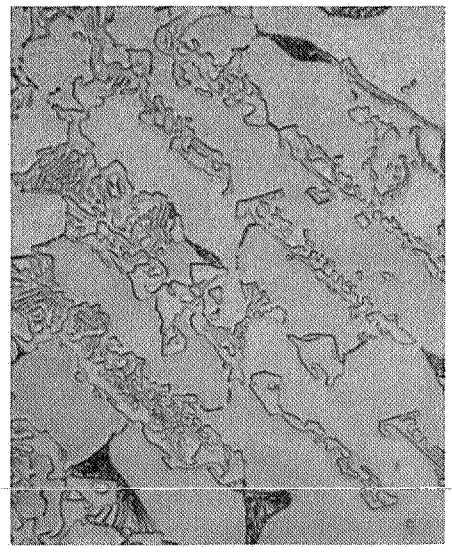

750X

c) As-cast

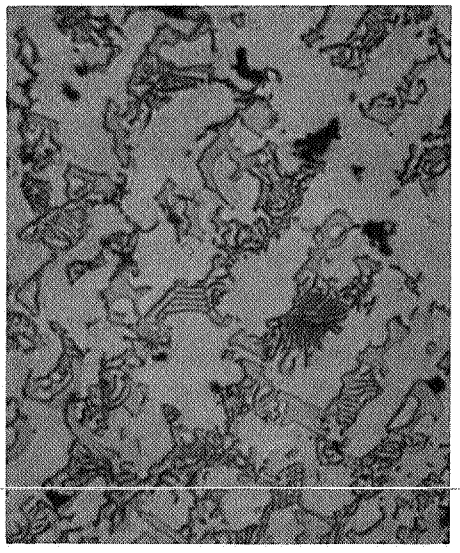

750X

d) Tested

Figure 4. Co-35W-3Cr-0.5C-0.1B, from gage section of stress rupture specimens.

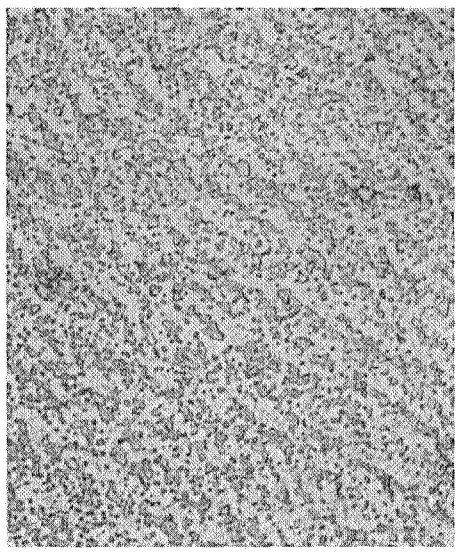

100X

a) As-cast

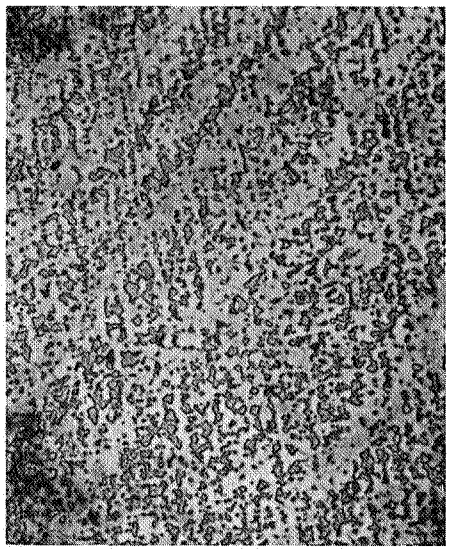

100X

b) Tested

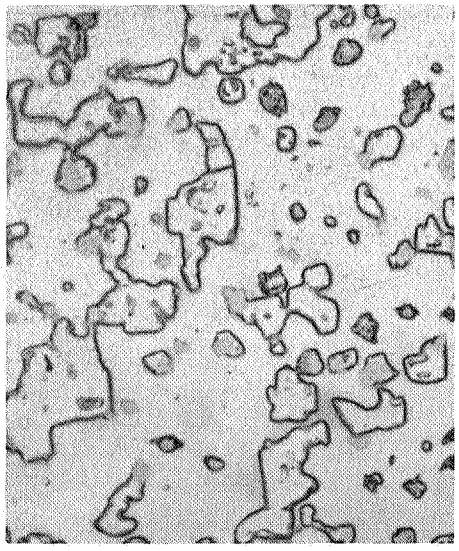

750X

c) As-cast

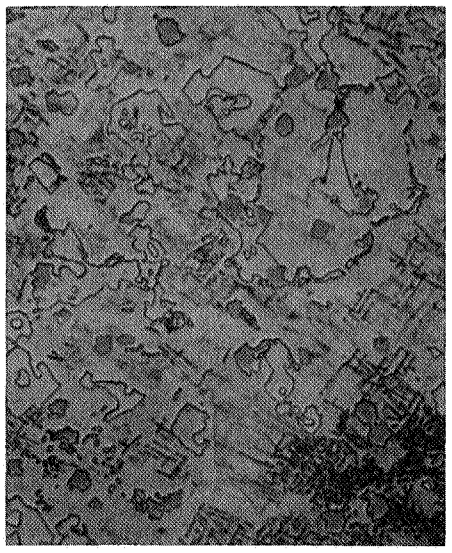

750X

d) Tested

Figure 5. Co-35W-3Cr-2Zr-0.5C-0.1B, from gage section of stress rupture specimens.

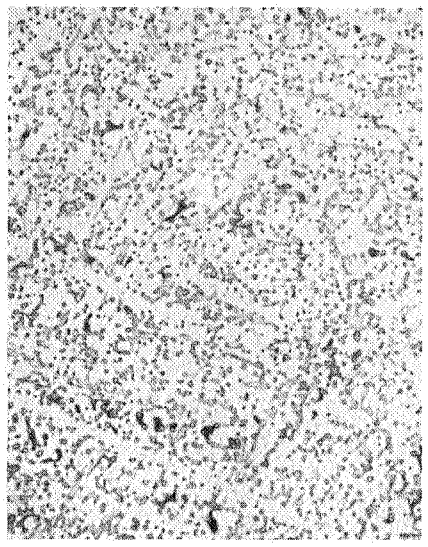

100X

a) As-cast

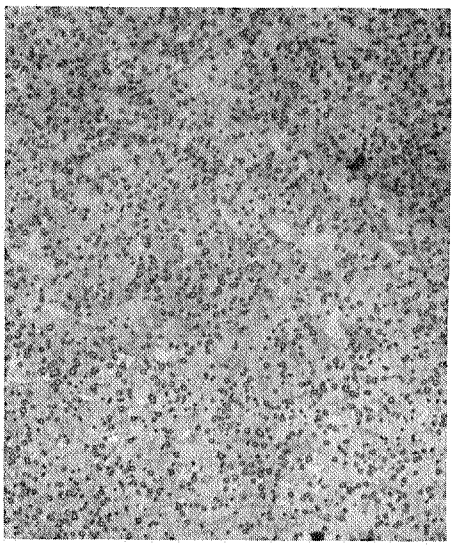

100X

b) Tested

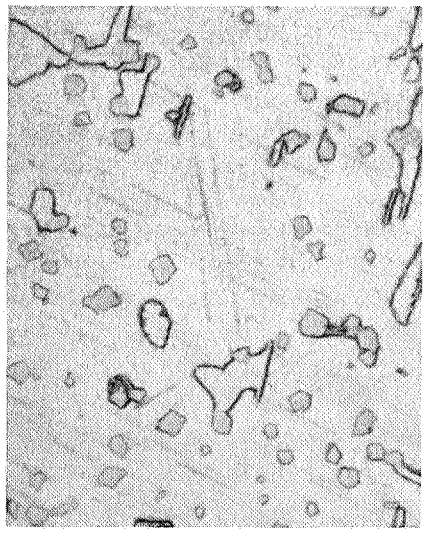

750X

c) As-cast

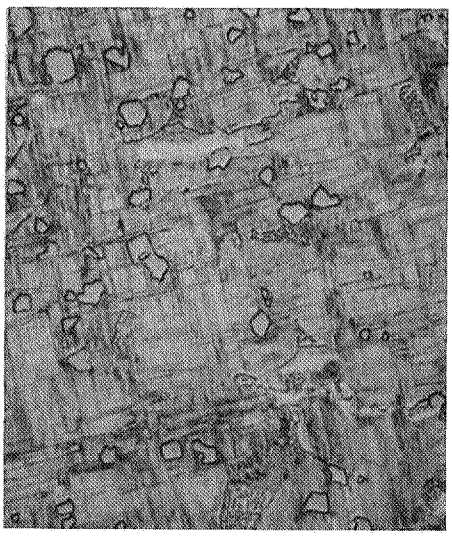

750X

d) Tested

Figure 6. Co-35W-3Cr-2Ti-0.5C-0.1B, from gage section of stress rupture specimens.

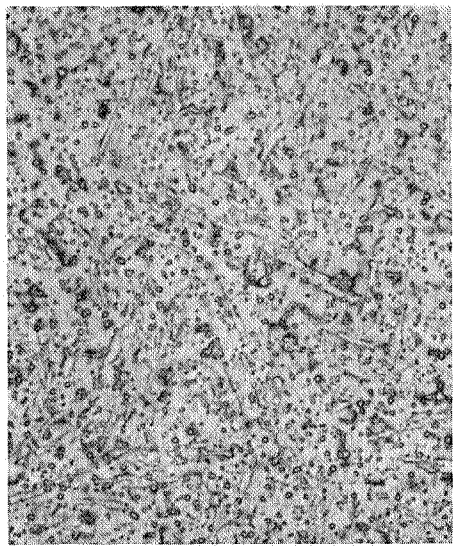

100X

a) As-cast

100X

b) Tested

750X

c) As-cast

750X

d) Tested

Figure 7. Co-35W-3Cr-2Ti-2Zr-0.5C-0.1B, from gage section of stress rupture specimens.

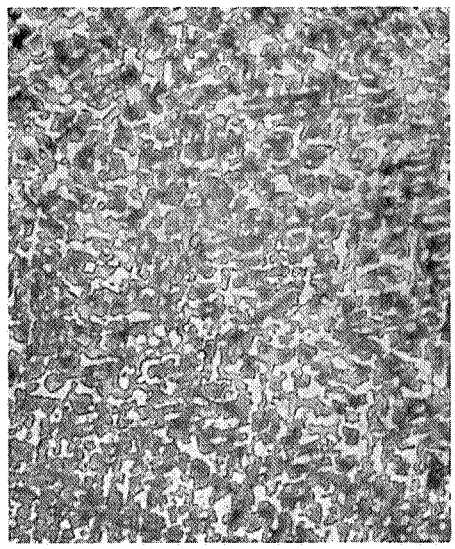

100X

a) As-cast

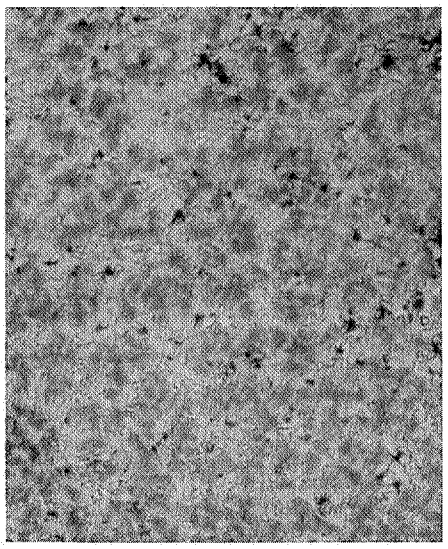

100X

b) Tested

750X

c) As-cast

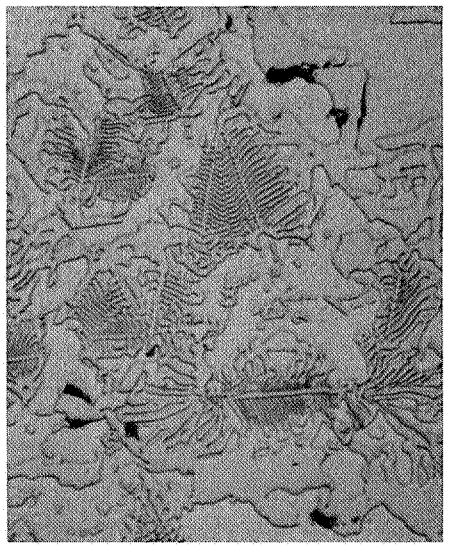

750X

d) Tested

Figure 8. Co-35W-3Cr-1C-0.1B, from gage section of stress rupture specimens.

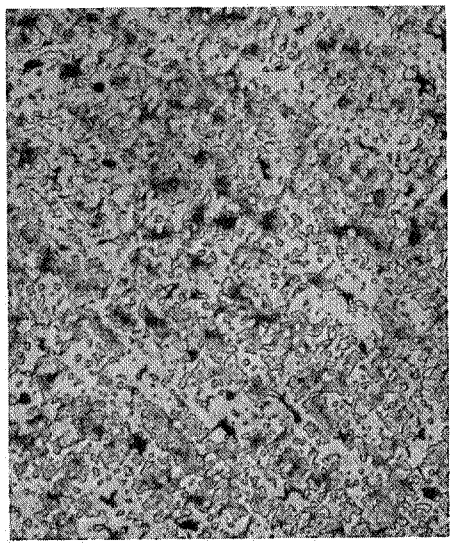

100X

a) As-cast

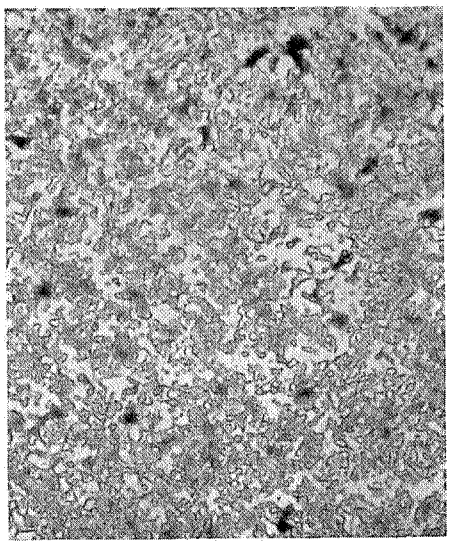

100X

b) Tested

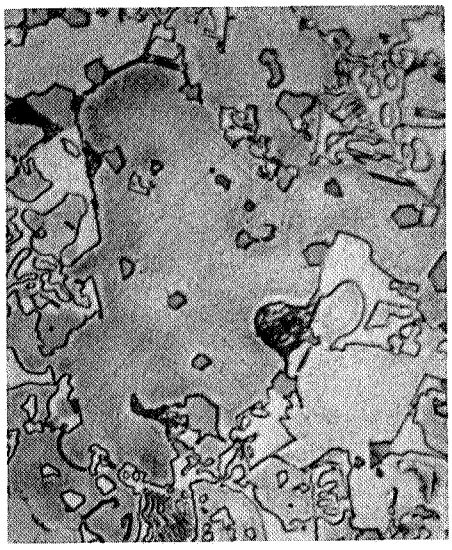

750X

c) As-cast

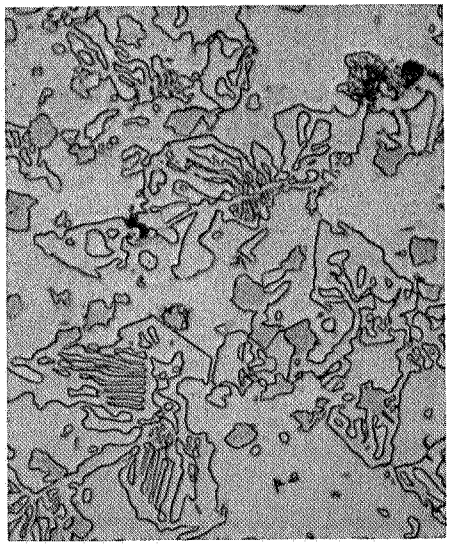

750X

d) Tested

Figure 9. Co-35W-3Cr-2Zr-1C-0.1B, from gage section of stress rupture specimens.

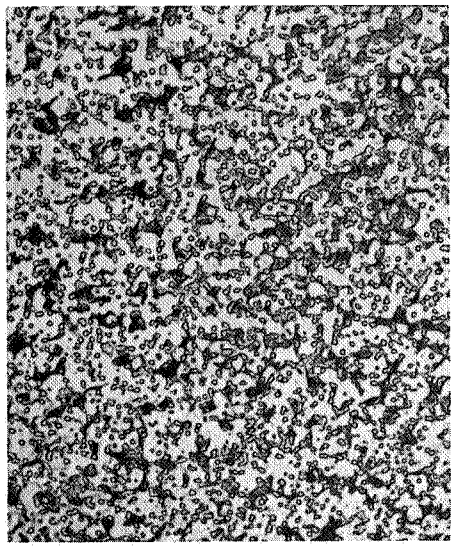

100X

a) As-cast

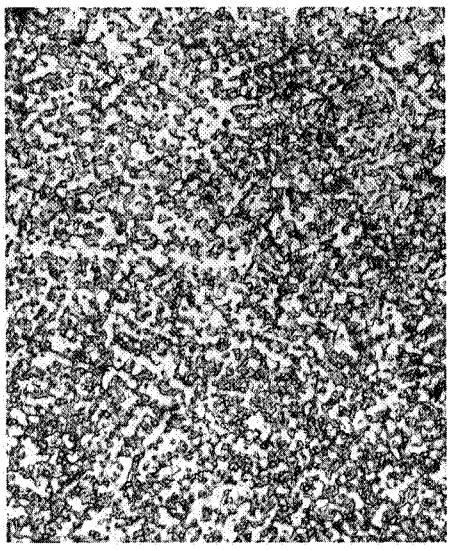

100X

b) After-testing

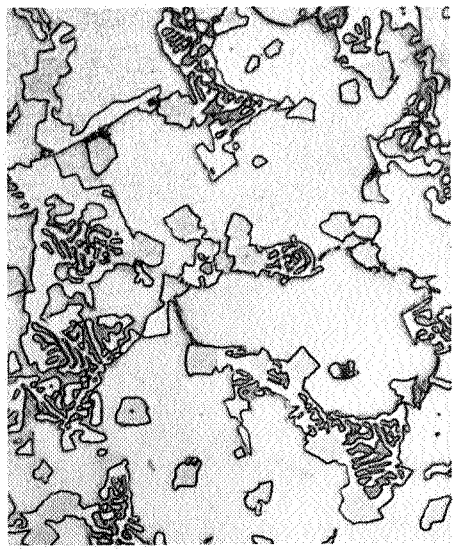

750X

c) As-cast

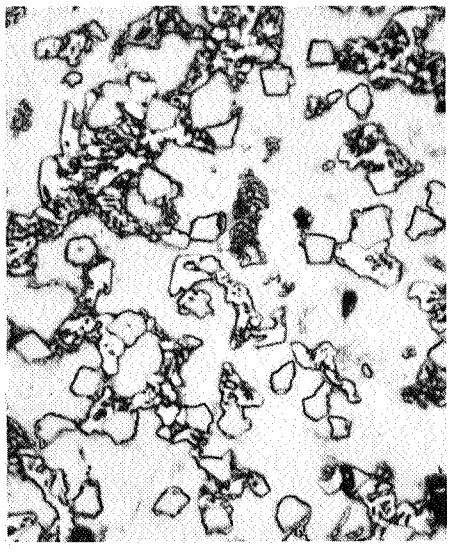

750X

d) After-testing

Figure 10. Co-35W-3Cr-2Ti-1C-0.1B, from gage section of stress rupture specimens.

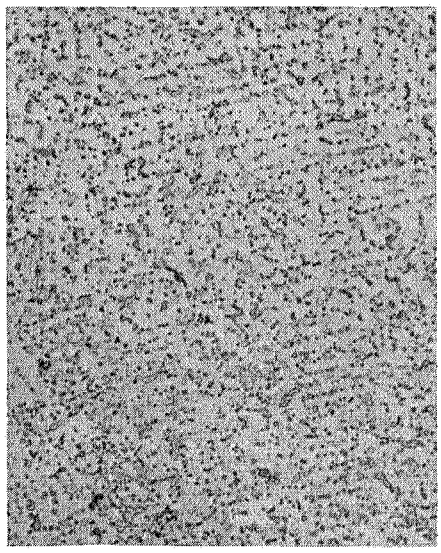

100X

a) As-cast

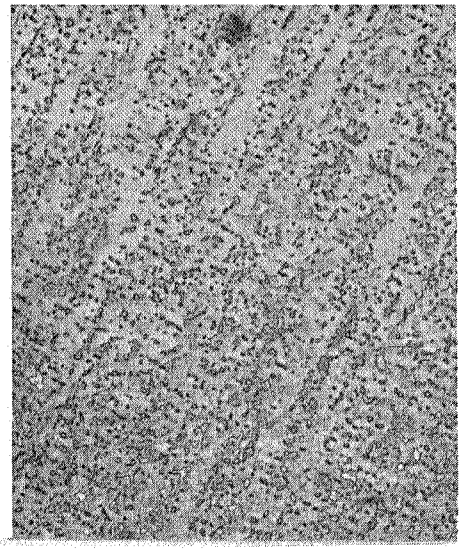

100X

b) After-testing

750X

c) As-cast

750X

d) After-testing

Figure 11. Co-35W-3Cr-1Ti-1Zr-0.5C-0.1B, from gage section of stress rupture specimens.

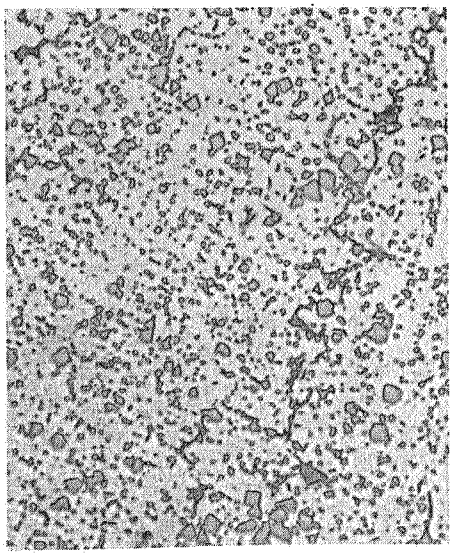

100X

a) As-cast

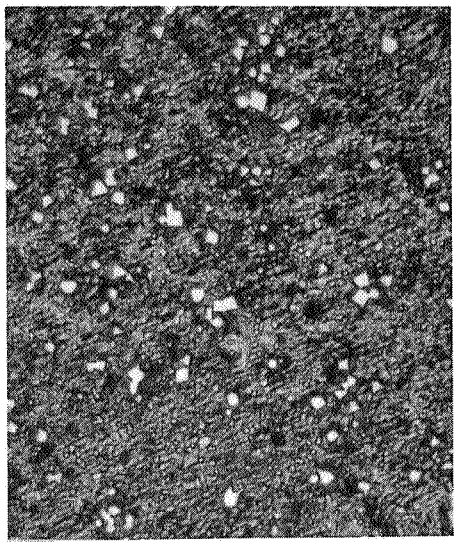

100X

b) After-testing

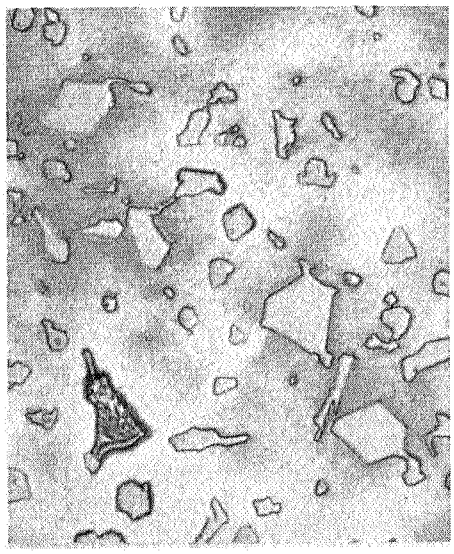

750X

c) As-cast

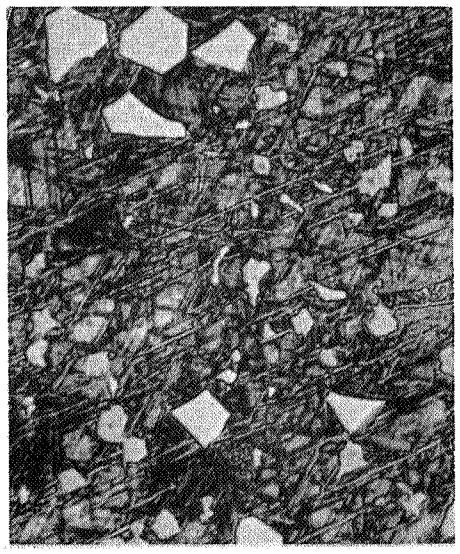

750X

d) After-testing

Figure 12. Co-35W-3Cr-2Ti-2Zr-1C-0.1B, from gage section of stress rupture specimens.

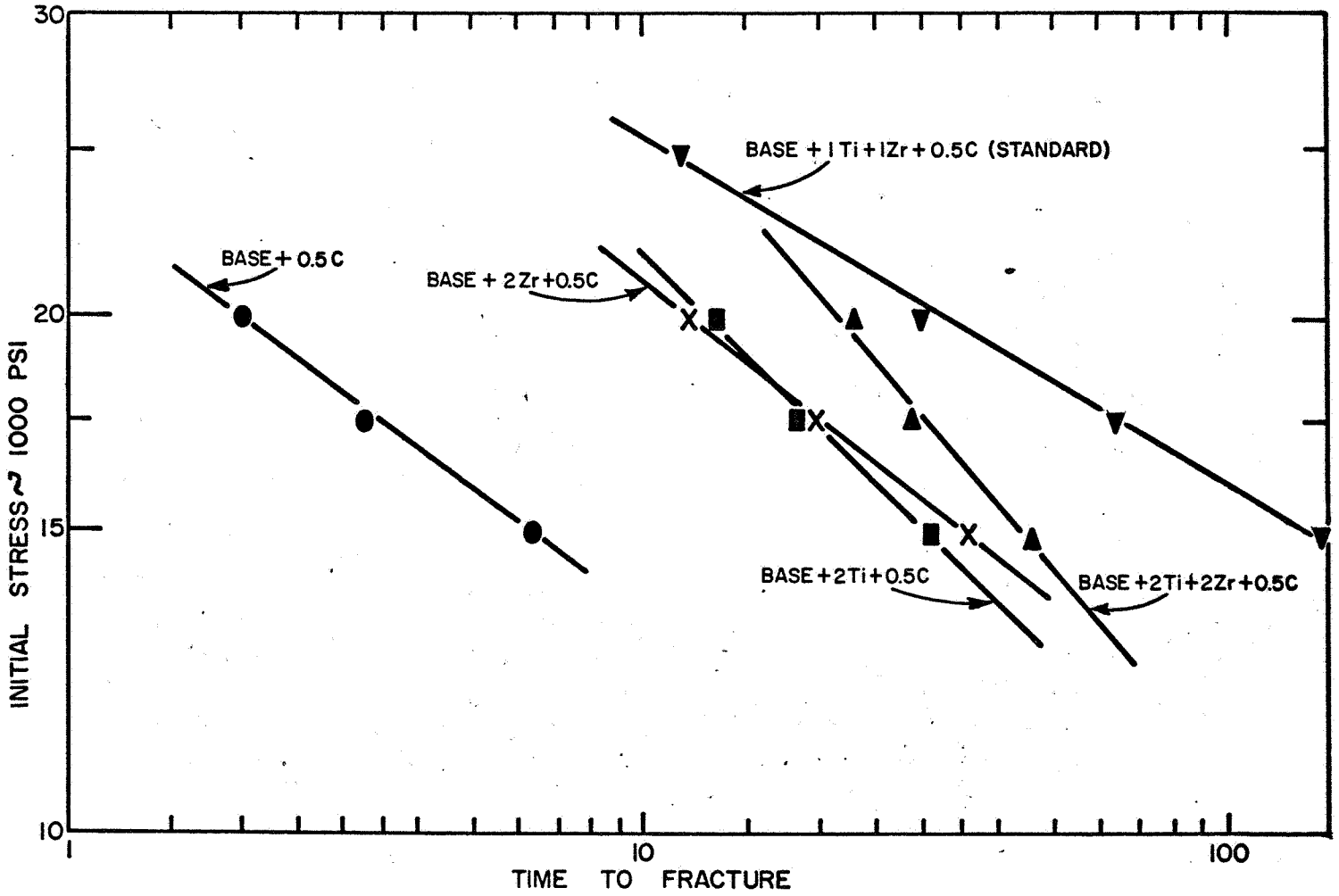

FIG. 13 : EFFECT OF Ti AND Zr ADDITIONS ON A Co – 35W – 3Cr – .5C BASE ALLOY (TESTED AT 1850°F IN AIR).

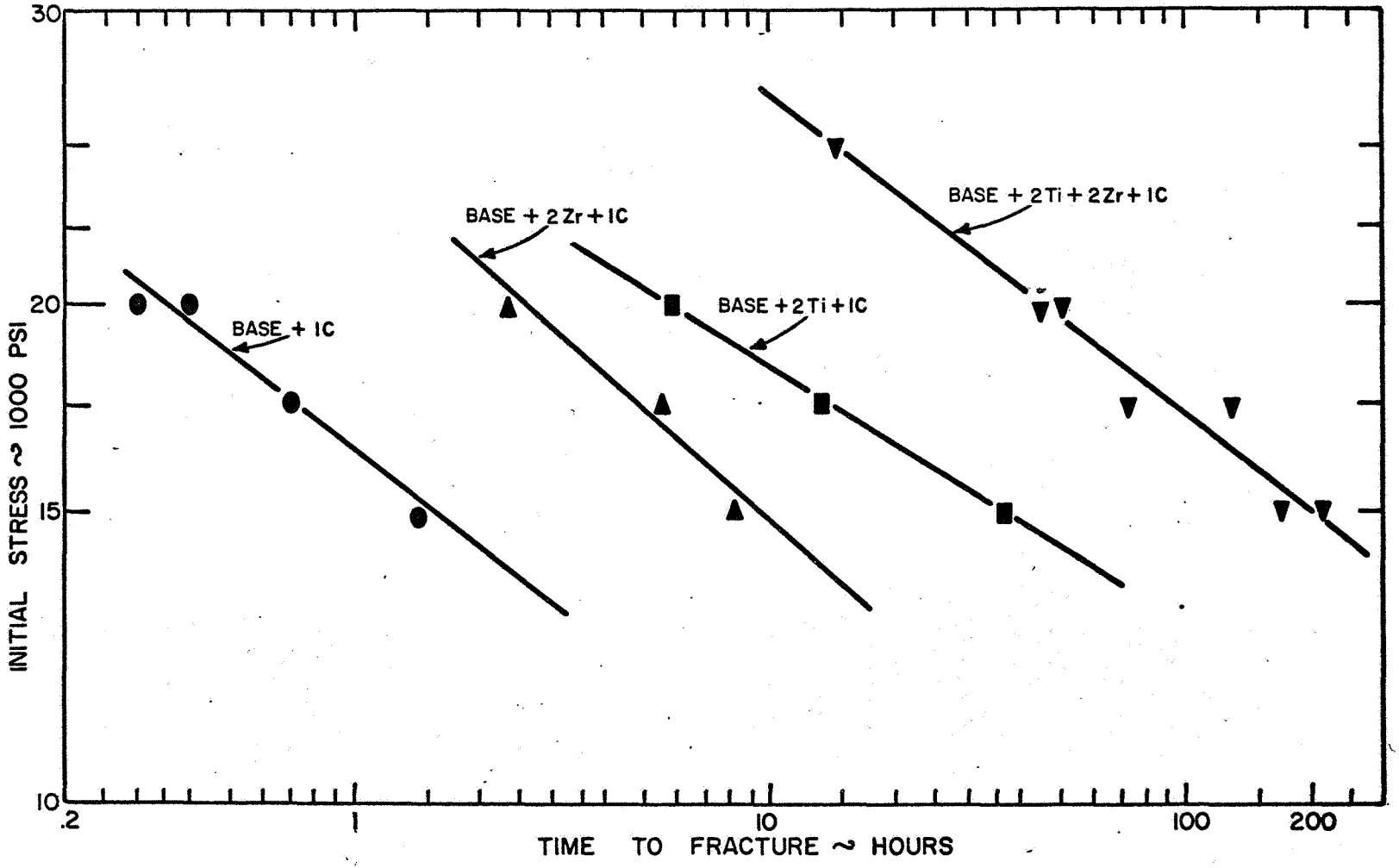

FIG. 14 : EFFECT OF Ti AND Zr ADDITIONS ON A Co – 35W – 3Cr – 1C BASE ALLOY (TESTED AT 1850°F IN AIR).

a) Conventional

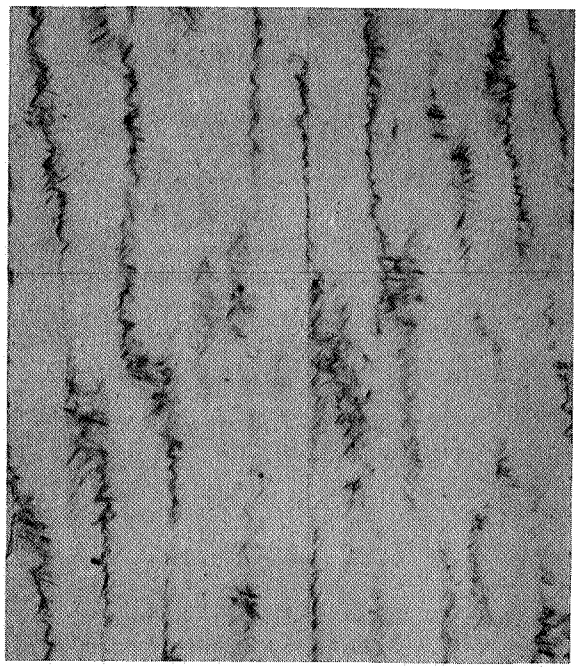

b) Directionally Solidified (vertically)

Figure 15. Co-35W-.05Zr from gage sections of stress rupture specimens, 100X.

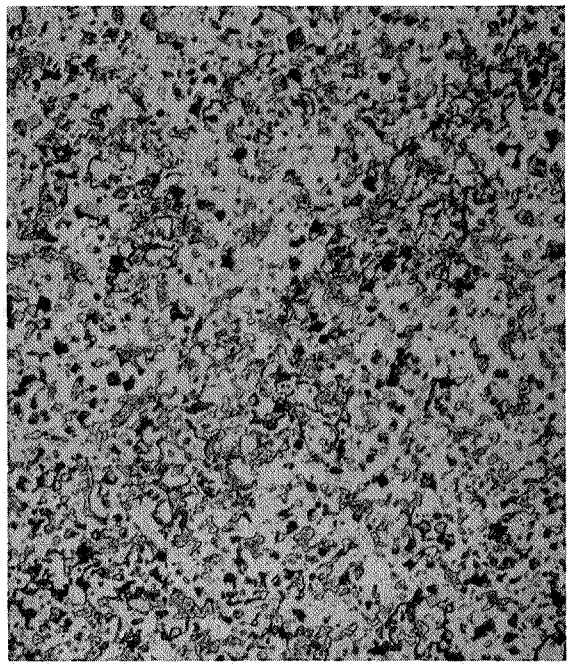

a) Conventional

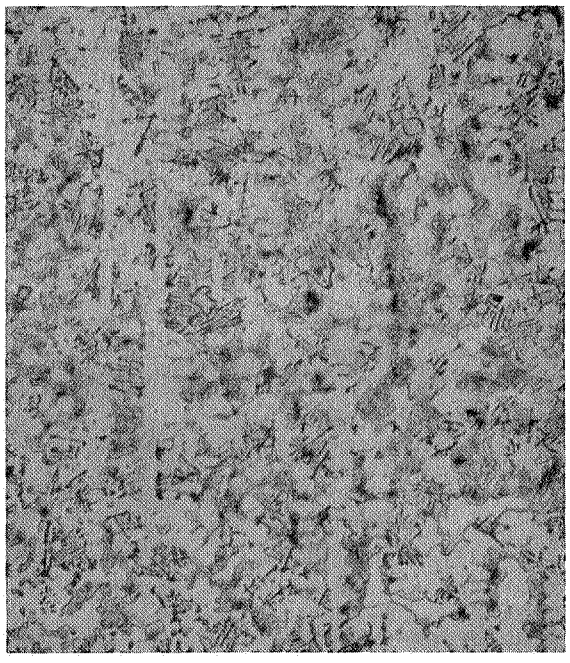

b) Directionally Solidified (vertically)

Figure 16. Co-35W-3Cr-2Ti-2Zr-1C-.1B from gage sections of stress rupture specimens, 100X.

a) Conventional

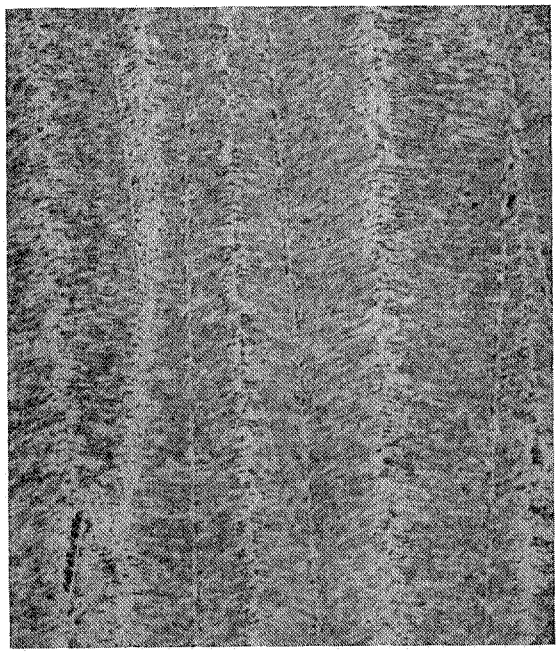

b) Directionally Solidified (vertically upward)

Figure 17. Co-45W-.05Zr from gage sections of stress rupture specimens, 100X.

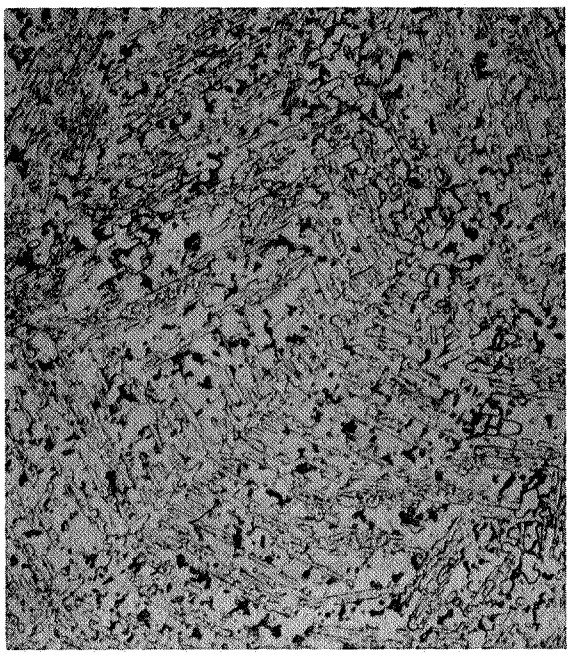

a) Conventional

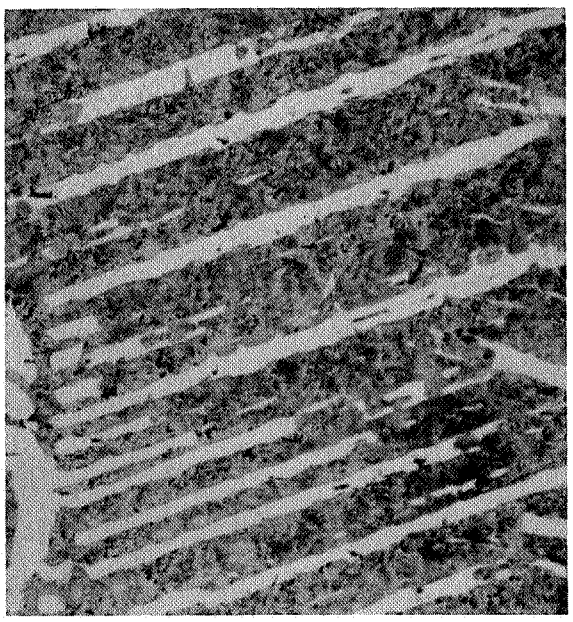

b)* Directionally Solidified (vertically upward)

Figure 18: Co-45W-.75-.75-.25-.1B from gage sections of stress rupture specimens, 100X. (*after testing).

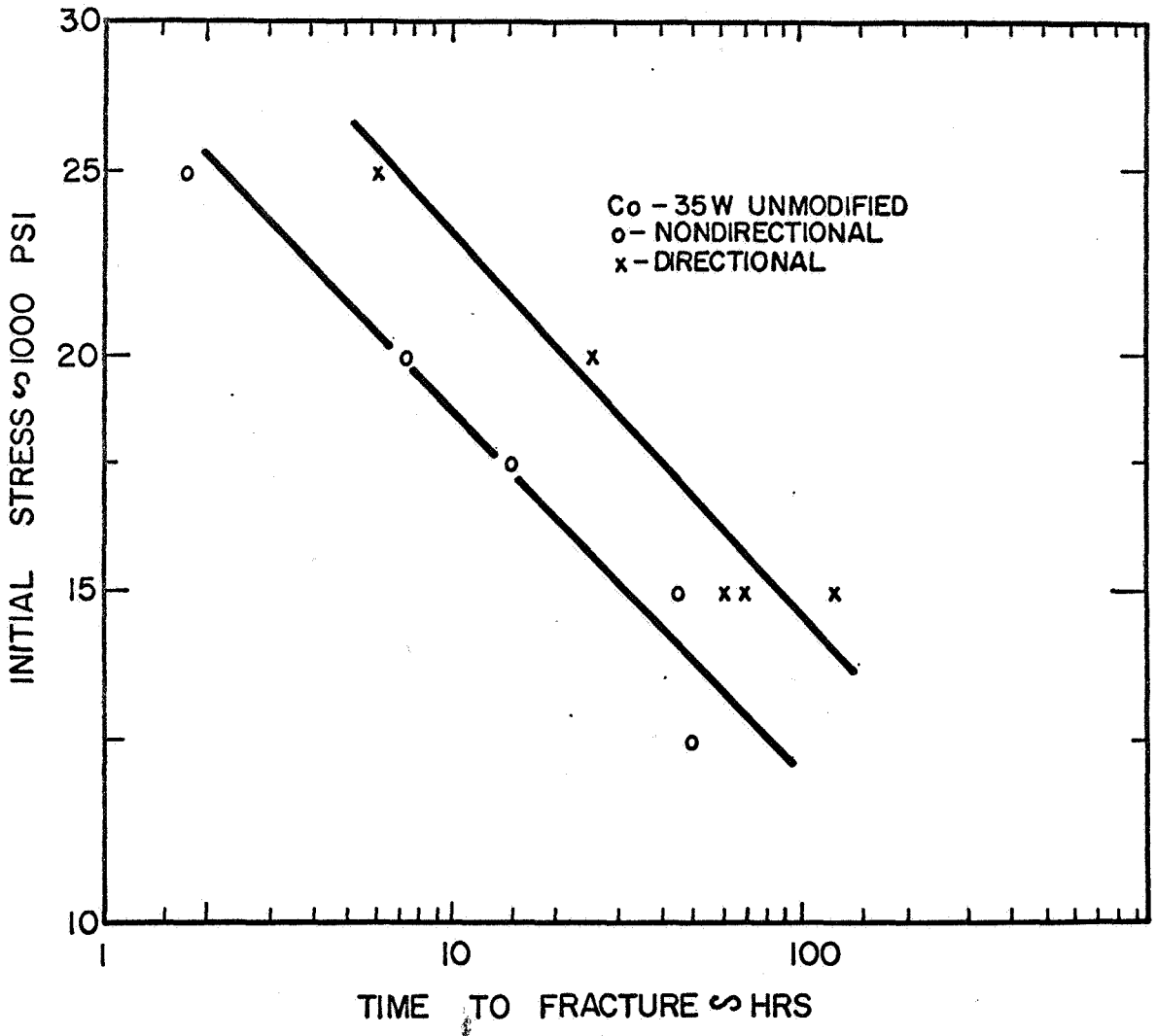

FIGURE 19: INFLUENCE OF CAST STRUCTURE ON STRESS RUPTURE LIFE OF Co-35 W, 0.05Zr. (TESTED IN AIR AT 1800° F)

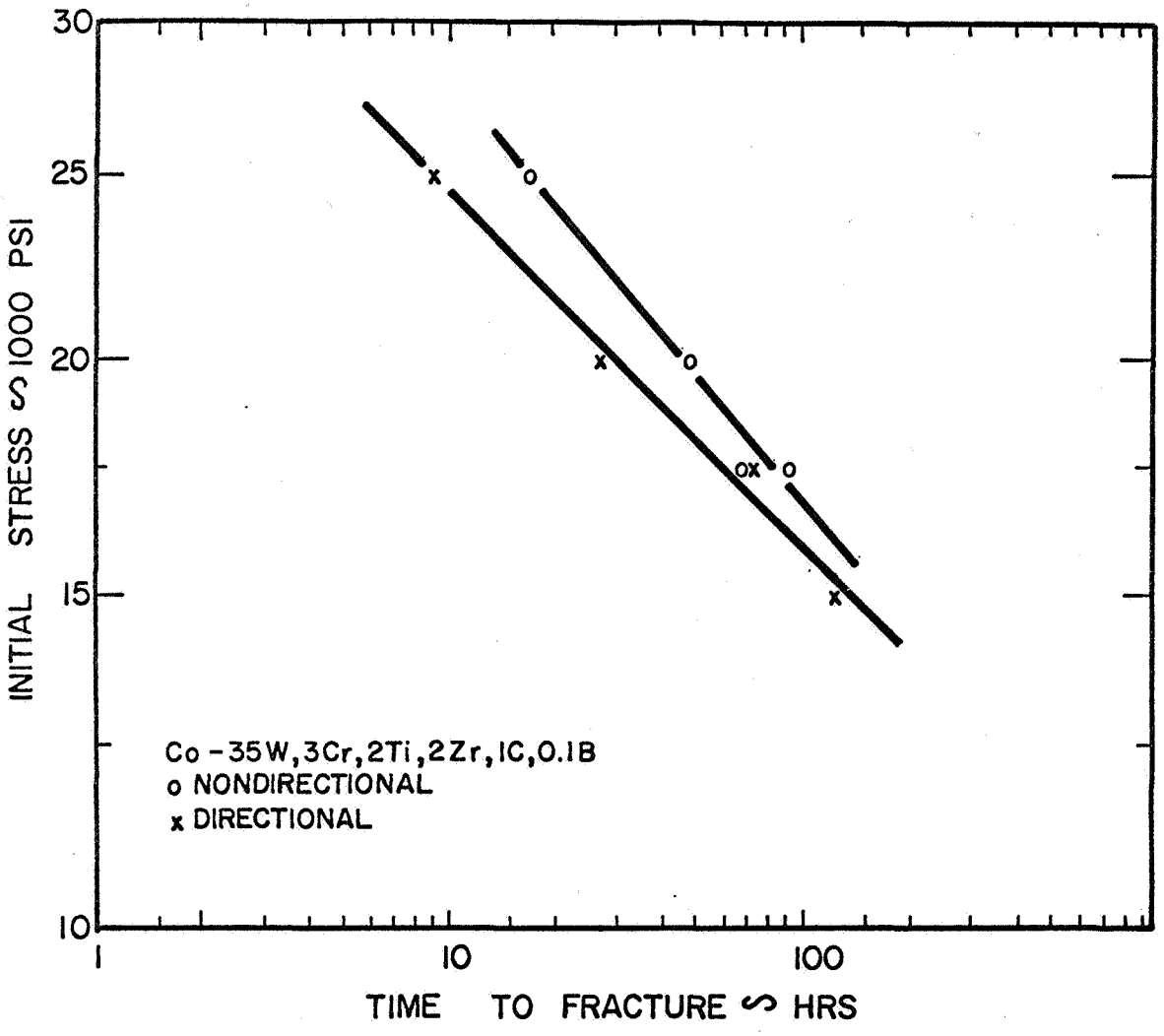

FIGURE 20: INFLUENCE OF CAST STRUCTURE ON STRESS RUPTURE LIFE OF Co-35W,3Cr,2Ti,2Zr,1C,0.1B. (TESTED IN AIR AT 1850°F)

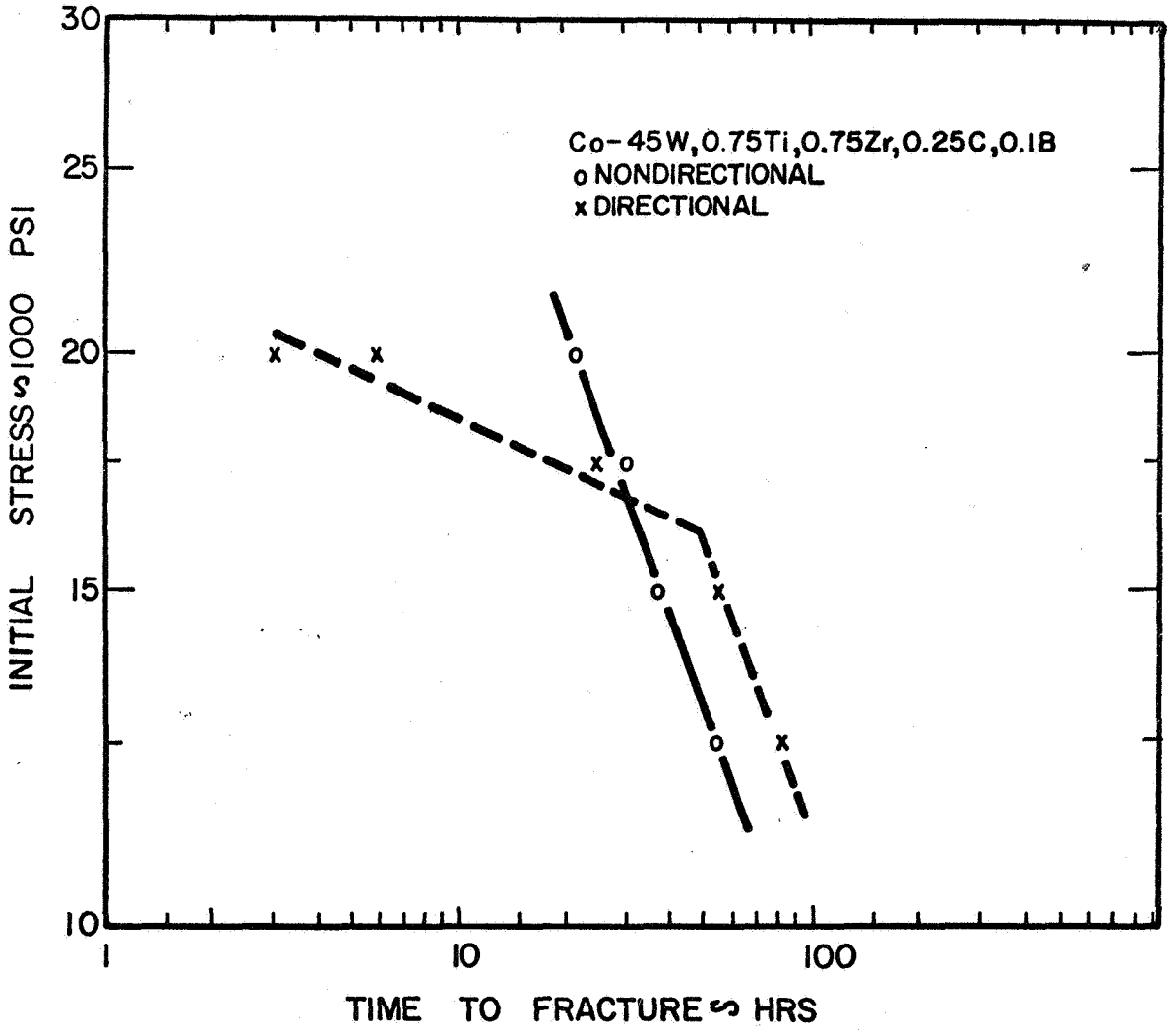

FIGURE 21: INFLUENCE OF CAST STRUCTURE ON STRESS RUPTURE LIFE OF Co-45W,0.75Ti,0.75Zr,0.25C,0.1B. (TESTED IN AIR AT 1800°F)

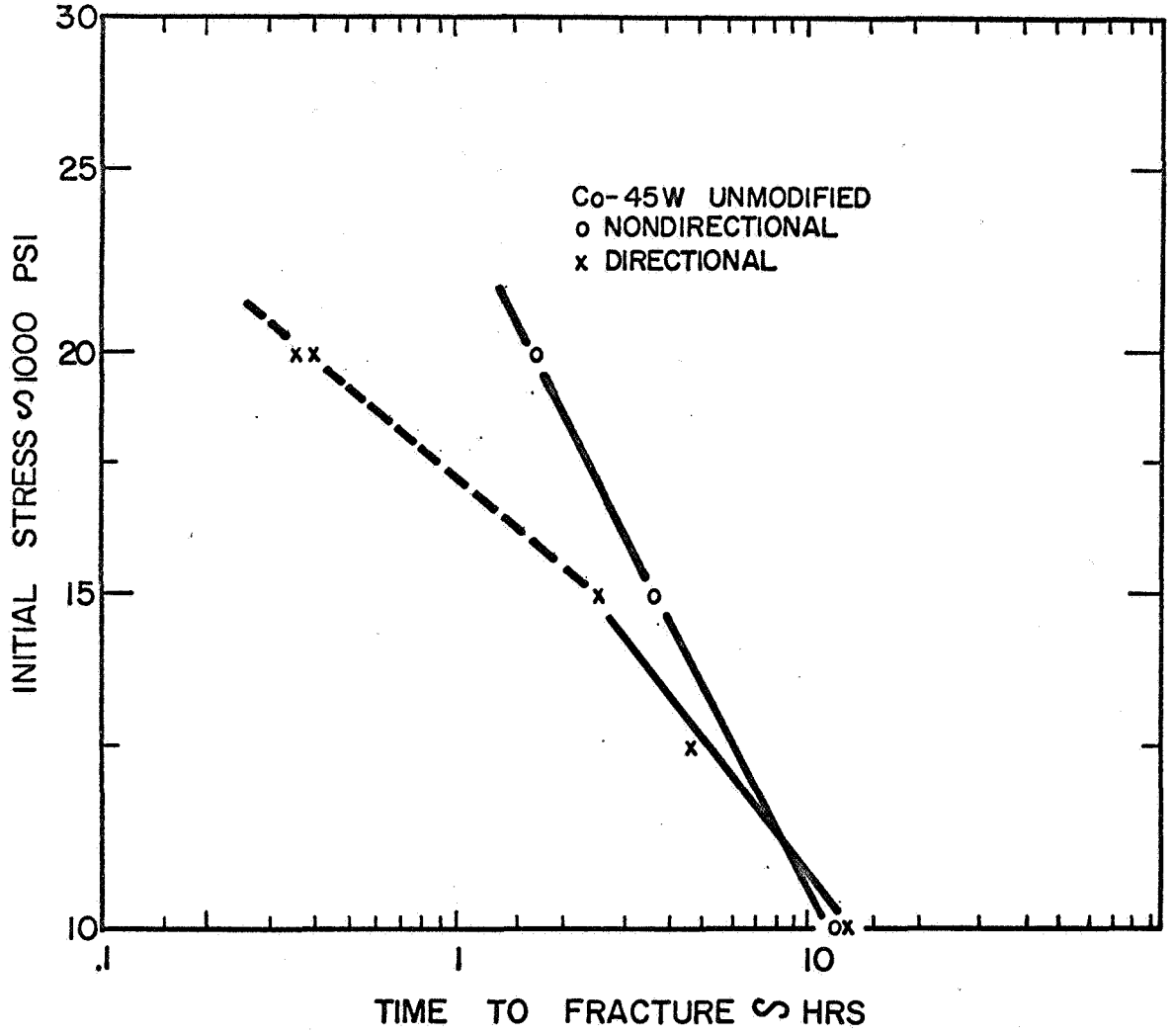

FIGURE 22: INFLUENCE OF CAST STRUCTURE ON STRESS RUPTURE LIFE OF Co-45W, 0.05Zr. (TESTED IN AIR AT 1800° F)

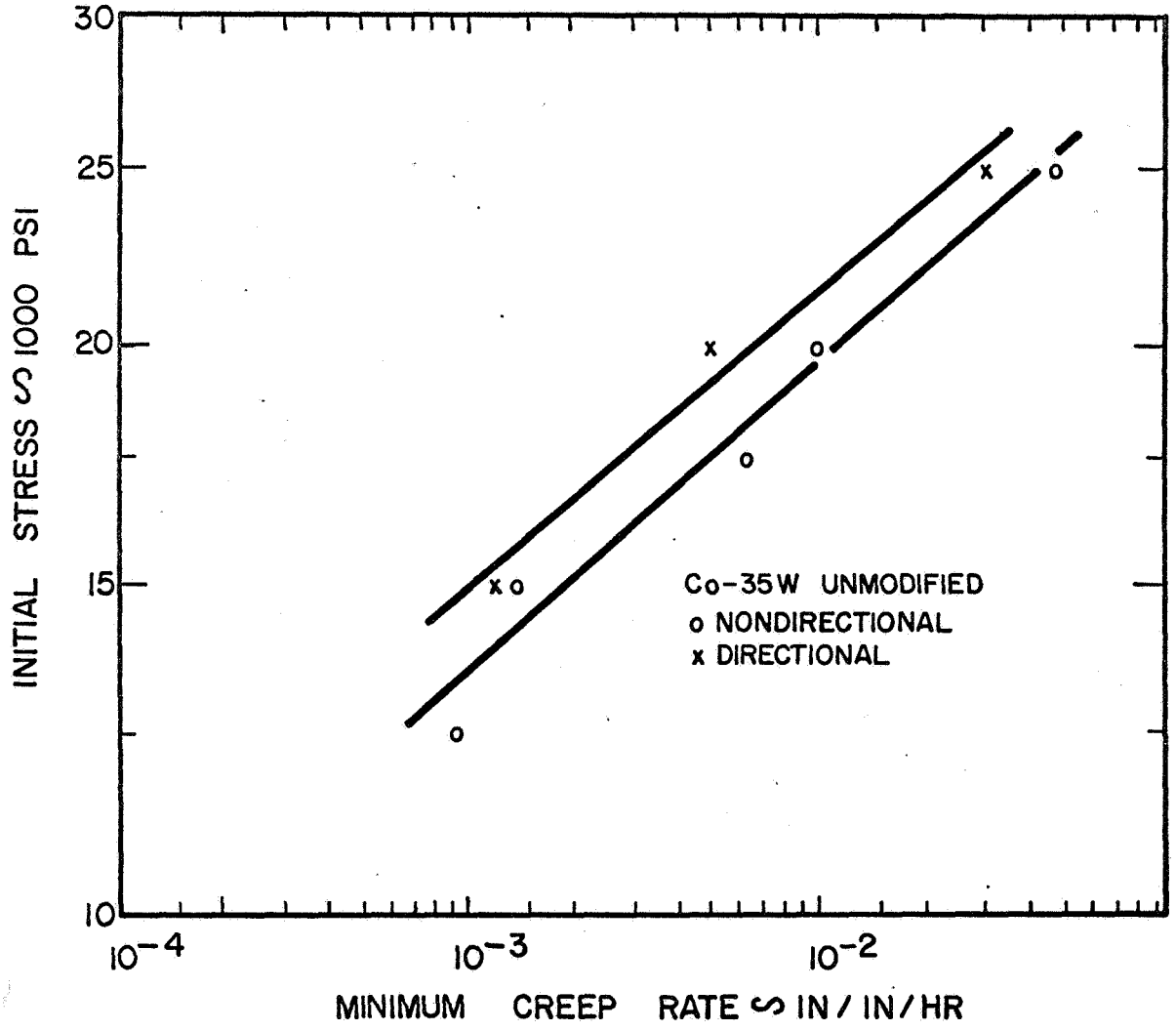

FIGURE 23: INFLUENCE OF CAST STRUCTURE ON MINIMUM CREEP RATE OF Co-35W, 0.05Zr. (TESTED IN AIR AT 1800°F)

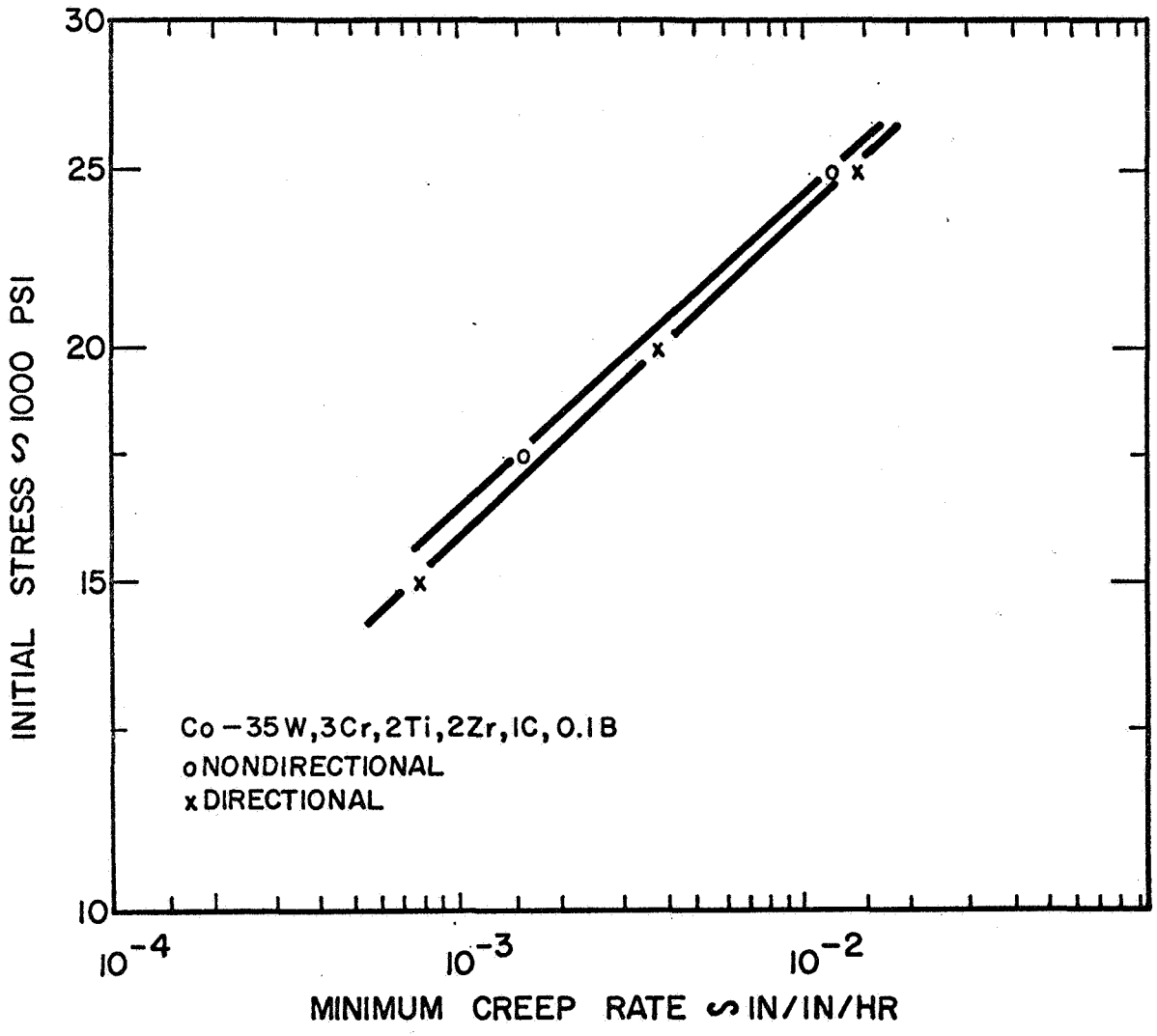

FIGURE 24: INFLUENCE OF CAST STRUCTURE ON MINIMUM CREEP RATE OF Co-35W,3Cr,2Ti,2Zr,1C,0.1B. (TESTED IN AIR AT 1850°F)

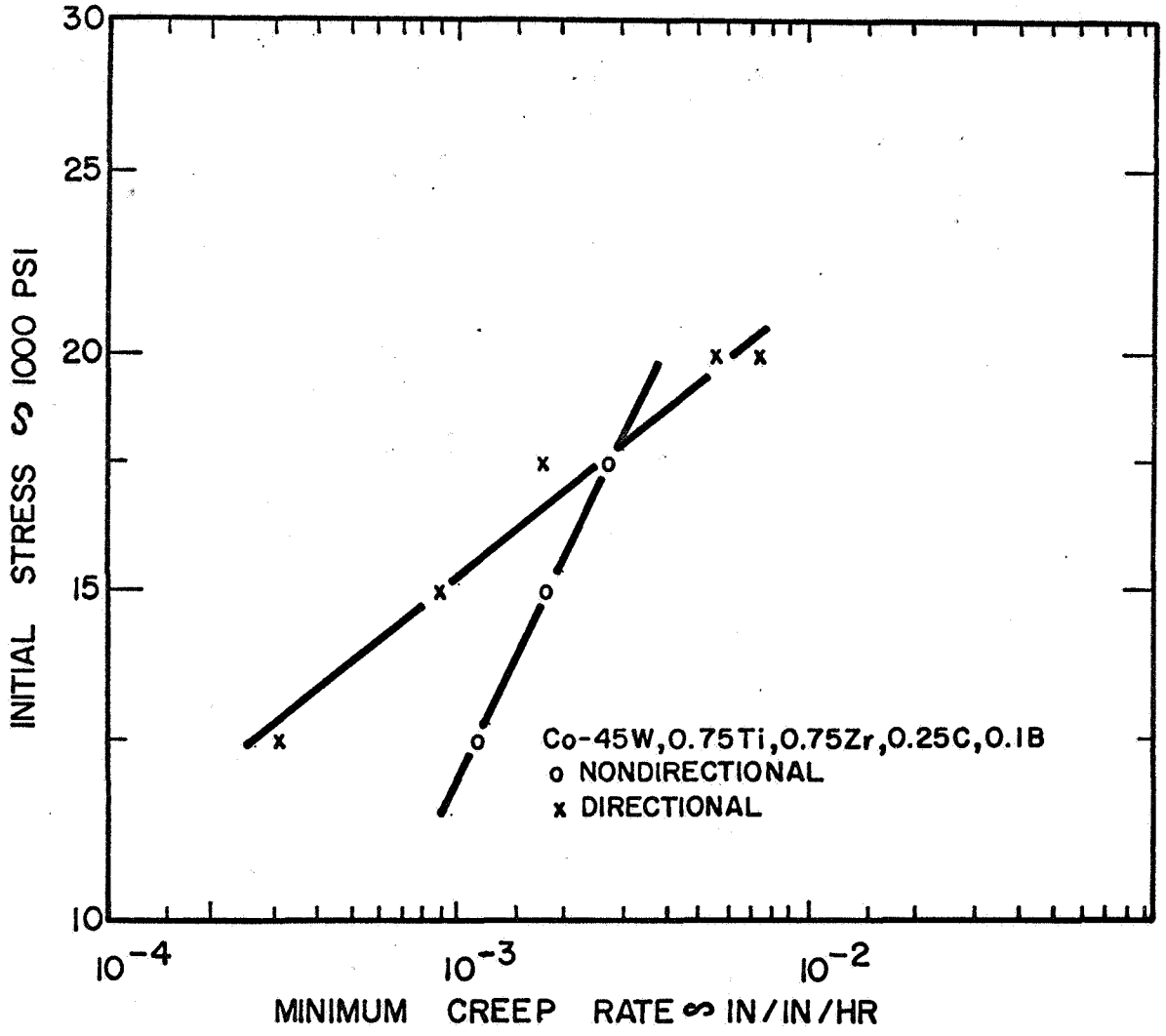

FIGURE 25: INFLUENCE OF CAST STRUCTURE ON MINIMUM CREEP RATE OF Co-45W,0.75Ti,0.75Zr,0.25C, 0.1B. (TESTED IN AIR AT 1800°F)

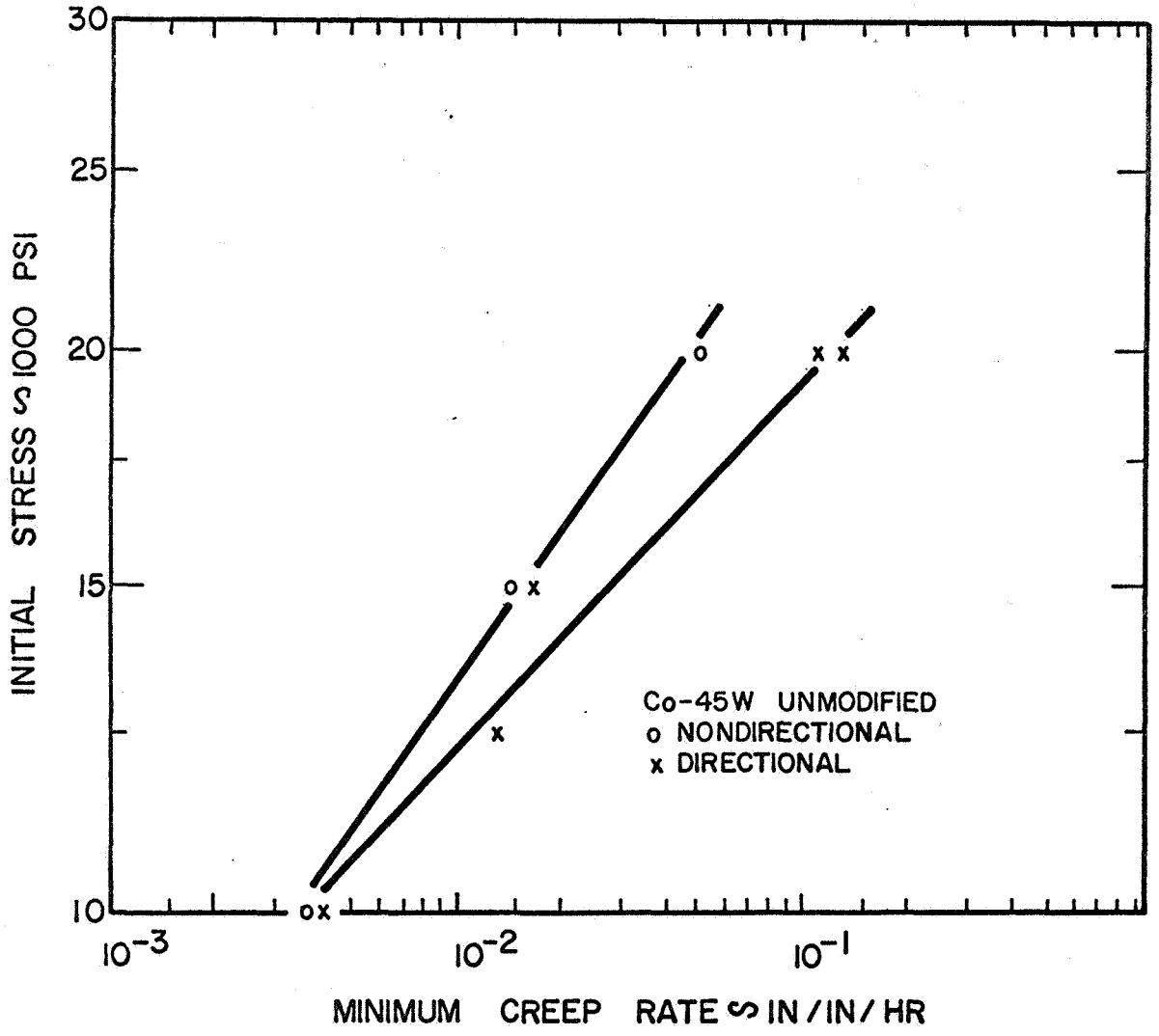

FIGURE 26: INFLUENCE OF CAST STRUCTURE ON MINIMUM CREEP RATE OF Co-45W, 0.05Zr. (TESTED IN AIR AT 1800° F)